Coumarin Derived Efficient Fluorescent Probe for Trace Level Determination of Hg (II) and Pb(II) in Environmental Samples: Experimental and Computational Studies

Dr. Subarna Guha

Faculty of Chemistry, Central Institute of Plastic Engineering and Technology, Haldia, West Bengal, India

Abstract : **A coumarin based efficient fluorescent probe selective for Hg^{2+} and Pb^{2+} ions was synthesized by coupling 6-amino-coumarin with 2-hydroxy naphthaldehyde. The probe and its metal complexes were well characterized by different spectroscopic techniques. The probe could detect up to 1µM Hg^{2+} and Pb^{2+} in aqueous methanol solution. The method showed linearity up to 10 µM for both Hg^{2+} and Pb^{2+}. Interference from other common cations is almost negligible. The probe showed a strong binding to Hg^{2+} and Pb^{2+} ions as evident from their binding constant values (2.2×10^4 and 1.4×10^4 respectively) estimated by Benesi-Hildebrand method. Computational studies (*Ab-initio*, Hartree Fock) indicated a molecular level interaction between the probe and Hg^{2+} and Pb^{2+} ions.**

Keywords: **Fluorescence, coumarin- naphthalene hybrid, Hg^{2+}, Pb^{2+}, environmental samples.**

I. INTRODUCTION

Hg^{2+} and Pb^{2+} ions are the most hazardous toxic heavy metal ions. Even the low dose exposure of mercury may lead to digestive, heart, stomach, kidney and especially neurological diseases [1-2]. Several analytical techniques for the determination of mercury ions in various real samples have been reported which include spectrophotometry [3-4], neutron activation analysis [5], anodic stripping voltammetry [6], X-ray fluorescence spectrometry [7], inductively coupled plasma mass spectrometry [8-11], electrothermal atomic absorption spectrometry [12-13] atomic fluorescence spectrometry [14] and cold vapor atomic absorption spectrometry [15]. Fluorescent chemosensors using chromoionophores [16] or polymers [17] have also been reported for Hg^{2+} detection. On the other hand, the fluorescence sensing method is nowadays a very efficient and popular method for low level monitoring of Hg^{2+} [18 - 25] due to its operational simplicity, high selectivity, sensitivity, rapidity, nondestructive methodology and direct visual perception [26-31].

The cumulative poisoning effect of lead causes hematological damage, anemia, kidney malfunctioning, brain damage, sore muscles, fatigue, irritation, and disturbances in the central nervous system [32]. The organic derivatives of lead are highly toxic because of the ease of their absorption by the body through skin and mucus membranes [33]. Although very few fluorescent Pb(II) sensors [34- 42] have been reported so far but work in this field is highly demanding and deserves much attention.

On the other hand, coumarin derivatives are well known to have diverse applications such as anticoagulants, spasmolytics, anticancer drugs or as plant growth regulating agents [32, 43-44]. Coumarin and its derivatives [45-46] possess antibacterial [47], antithrombotic and vasodilatory [48], antimutagenic [49], lipoxygenase and cyclooxygenase inhibition [50-51] properties. They act as scavenger of reactive oxygen species [52-53].

Thus, from the above discussion, it was evident that applications of coumarin derivative as fluorescent probe for trace level determination of Hg^{2+} and Pb^{2+} ions in aqueous solution might be an important area of research.

Herein we present the synthesis, characterization, and application of a new Hg^{2+} and Pb^{2+} selective fluorescent sensor by anchoring naphthalene derivative to the coumarin backbone.

II. EXPERIMENTAL

Materials and Methods

2-hydroxynapthaldehyde and coumarin were purchased from Aldrich Chemical Co. (USA) and S.D. Fine Chem. Ltd. (India) respectively. All other chemicals were of reagent grade and used without further purification. Spectroscopic grade solvents and Milli-Q 18Ω water were used throughout all the experiments. Stock solution of Pb(II) (1000 mg L^{-1} in 3% $HNO_3$was obtained from **SOLUTIONS plus inc.** (Missouri, USA) which was tested *vs.* NIST SRM # 3108a. Then the solution was diluted 20 times for our practical work. All the working solutions were prepared by appropriate dilution with deionised water. Glass apparatus were soaked with 4 mol $L^{-1}HNO_3$ overnight and cleaned with double distilled (d. d.) water. Certified reference materials analyzed were standard reference material (SRM) 1573 tomato leaves

from National Bureau of Standards; pond sediment (NIES 2) and igneous rock (JR-1) from National Institute for Environmental studies, Japan.

Physical measurements

Microanalytical data (C, H and N) were collected on Perkin-Elmer 2400 CHNS/O elemental analyzer. Spectroscopic data were obtained using the following instruments: UV-vis. spectra by Perkin Elmer UV-vis. spectrophotometer model Lambda 25; FTIR spectra (KBr disk, 4000-450 cm^{-1}) by Perkin Elmer FT-IR spectrophotometer model RX-1; Mass spectra were recorded in QTOF Micro YA 263 mass spectrometer in ES positive mode. Thermo gravimetric analysis was performed on a Perkin Elmer TG/DTA lab system l (Technology by SII).^{1}H NMR spectra was recorded on Bruker (AC) 300 MHz. Fluorescence studies were carried at room temperature (298 K) in aqueous methanol solution (water: methanol = 1: 4, v/v) with a Hitachi F-4500 spectrofluorimeter. A domestic Samsung microwave oven (model CE2933) with a 2450 MHz frequency magnetron and 900W maximum power and a polytetrafluoroethylene (PTFE) reactor (115 mL internal volume, 1 cm cell wall thickness and hermetic screw caps) were used for digestion. Direct analysis of Pb^{2+} in road dust samples were performed using flame atomic absorption spectrometer (Varian A55, Australia) after microwave assisted digestion. Computational studies were carried out using Gaussian 03 software [54].

Synthesis of (6E)-6-((2-hydroxynaphthalen-3-yl)methyleneamino)-2H-chromen-2-one (L)

Scheme 1 showed the protocol for the synthesis of the probe. 6-Aminocoumarine (0.5 g, 3.1 mmol) was dissolved in 10 mL dry methanol and mixed with 10 mL dry methanol solution of 2-hydroxynapthaldehyde (0.5341g, 3.1 mmol). The mixture was refluxed for 4 h. slow evaporation of the solvent yielded a yellow color compound which was re-crystallized from methanol. Yield 90%; m. p. 190 ± 2 °C; ^{1}HNMR (300MHz, $CDCl_3$) (Fig.S1): δ (ppm): 6.48 (d, J = 9.55, 1H), 7.75 (d, J = 9.5, 1H), 7.37 (s, 1H), 7.38 (d, J = 8.65,1H), 8.63(S,1H), 8.26(s, 1H), 7.22 (s, 1H), 7.63 (d, 1H), 7.21 (m,1H), 7.3 (m,1H), 7.53 (d, 1H), 6.39 (s, 1H). QTOF – MS ES^+ (Fig.S2): $[M+H]^+$ =316; FTIR (KBr, cm^{-1}) (Fig.S3) ν(COO), 1721; ν(C=N), 1623; UV-vis. (λ_{max}, nm (ε, 10^3M^{-1} cm^{-1}, CH_3OH) 383(1.241), 363 (1.358), 253(21.43), 212(22.72). Microanalytical data, calculated for $C_{20}H_{13}NO_3$: C, 76.18; H, 4.16; N, 4.44, found: C, 75.95; H, 4.11; N, 4.43.

Synthesis of L- Hg^{2+} complex [HgL_2](Scheme2)

A 10 mL methanolic solution of $HgCl_2$ (0.025 g, 0.0923 mmol) was added slowly to a magnetically stirred 10 mL methanol solution of **L** (0.058 g, 0.1846 mmol). Stirring was continued for 2 h to get a clear solution. Slow evaporation the solvent yielded a brown compound which was re-crystallized from methanol. QTOF–MS ES^+ (Fig.S4) $[M+H]^+$ = 831.15. FTIR (KBr, cm^{-1}) (Fig. S5): ν(COO), 1717; ν(C=N), 1610, UV-vis. (λ_{max}, nm (ε, 10^3M^{-1} cm^{-1}, CH_3OH) 372 (1.7), 333 (1.56), 314 (1.73), 227 (8.25). Microanalytical data, for $C_{40}H_{24}HgN_2O_4$ C, 57.94; H, 2.92; N, 3.38, found: C, 57.76, H, 2.88, N, 3.37.

Synthesis of L-Pb^{2+} complex [$PbL(NO_3)_2$](Scheme 2)

A 10 mL solution of $Pb(NO_3)_2$ (0.025 g, 0.075mmol) in methanol was added slowly to a magnetically stirred 10 mL methanol solution of the **L** (0.047 g, 0.15 mmol). The mixture was stirred for another 2 h to have a clear solution. Slow evaporation of methanol yielded a very light brown color compound which was re-crystallized from methanol. QTOF–MS ES^+ (Fig.S6) $[M+H]^+$ = 647.08. FTIR (cm^{-1}) (Fig.S7): ν(COO), 1722; ν(C=N), 1615, UV-vis. (λ_{max}, nm (ε, 10^3M^{-1} cm^{-1}, CH_3OH) 367 (2.39), 333 (2.22), 315 (2.43), 227 (10.87). Microanalytical data, for $C_{20}H_{12}N_3O_9Pb$ C, 37.21; H, 1.87; N, 6.51, found: C, 37.09; H, 1.85; N, 6.49.

Measurement procedures

A 1×10^{-5} mol L^{-1} working solutions of Hg^{2+} and Pb^{2+} were obtained by serial dilution of their respective stock solutions. A 10^{-5} mol L^{-1} stock solution of **L** was prepared by dissolving appropriate amount of **L** in aqueous methanol (methanol: water = 4:1, v/v). Solutions of Hg^{2+} and **L** were mixed in different ratios for subsequent fluorescence measurements. Similar experiment was performed with Pb^{2+}. The fluorescence emission intensity was measured at 350 nm (λ_{em}) while excitation wavelength (λ_{ex}) was fixed at 253 nm. 1.00 cm quartz cell was used for fluorescence measurement.

III. RESULTS AND DISCUSSION

Spectral characteristics

Upon addition of Hg^{2+} and Pb^{2+} ions, emission intensities of **L** show a gradual decrease at 350 nm. (λ_{ex} = 253 nm and slit width 10/10 nm). The changes in the fluorescence emission intensities of **L** ([**L**] = 10^{-6} mol L^{-1}) as a function of externally added Hg^{2+} (from 0.2 μM to 10 μM) and Pb^{2+} ions (from 0.1 μM to 15 μM) were presented in Fig. 1 and Fig. 2 respectively.

The plots of emission intensities *vs* externally added Hg^{2+} and Pb^{2+} ions (inset of Fig.1 and Fig.2) reveal that after a certain amount of externally added Hg^{2+} ion and Pb^{2+} ion, there is no further change in the emission intensity of the system. Up to 10 times of the externally added Hg^{2+} ion and Pb^{2+} ion, we observed linearity. Thus, by making use of this linear relationship (inset of Fig.1 and Fig.2), one can easily determine the concentration of any unknown Hg^{2+} ion and Pb^{2+} ion in aqueous solution.

Job's plot (Fig. 3) showed the stoichiometry of the complexes formed between **L** and Hg^{2+} as **L**: Hg^{2+} = 2: 1(mole ratio) whereas for the **L**- Pb^{2+} (Fig.4) complex it was found as **L**: Pb^{2+} = 1: 1 (mole ratio). These compositions were in complete agreement with the mass spectra (Fig. S4 and Fig. S6) of the complexes.

Changes in the absorption spectra of **L** with externally added Hg^{2+} and Pb^{2+} in aqueous methanol (methanol: water = 4: 1, v/v, [L] = 10^{-4} mol L^{-1}) were presented in Fig. S8. The UV–vis spectra of the Schiff bases contained hypochromic absorption bands in the ultraviolet region of the spectra corresponding to the π-π* transitions of the aromatic rings and of the conjugated system arising from the imine and coumarin moieties. Low intensity, broad bands, with absorption maxima at ca. 430 nm, were assigned to forbidden n-π* transitions associated with the azomethine group.

In the IR spectra of the Hg^{2+} and Pb^{2+} complexes the $\upsilon_{C=N}$ stretching vibration associated with the imine functional group of the ligand was shifted to a lower wavelength compared to that in the corresponding free ligand, indicating that coordination to the Hg^{2+} and Pb^{2+}ion occurs via the imine nitrogen. The $\upsilon_{C=O}$ stretching vibration of the carbonyl function in the lactone ring of the free ligands appeared as a strong sharp band in 1720 cm^{-1}. In the spectrum of most of the complexes, the position of this band remained largely unchanged, suggesting that the lactone carbonyl oxygen is not involved in coordination to the metal. For Pb^{2+} complexes stretching vibration at 1373 cm^{-1} denoted presence of nitro group.

Calculation of binding constant

Binding constant (K) values of **L** for Hg^{2+} and Pb^{2+} ions in aqueous methanol were determined (Fig.5 and Fig.6) using the Benesi- Hildebrand, equation, $I_0 / (I_0\text{-}I) = 1/A + 1/KA \cdot 1/[Q]$, where I_0 is the fluorescence intensity of the free **L**, I is the fluorescence intensity of the complex, [Q] is [Hg^{2+}] and [Pb^{2+}], A is a constant and K is the binding constant. Fairly strong binding between **L** and [Hg^{2+}] or [Pb^{2+}] was observed from their respective binding constant values *viz.* 2.2 x10^4 M^{-1} for [Hg^{2+}] and 1.4 x 10^4 M^{-1} for [Pb^{2+}].

Selectivity

The selectivity of **L** for Hg^{2+} and Pb^{2+} over 3d metal ions was examined in aqueous methanol solution. Fig.7 indicated that Hg^{2+} and Pb^{2+} quenched the fluorescence intensity of **L** to the maximum extent whereas 3d metal ions could not achieve to that extent.

In a competitive environment, with ternary mixtures (**L** + Hg^{2+} / Pb^{2+} + M^{n+} = 1:1:1, mole ratio), interferences of 3d metal ions on the emission intensity of the [**L**-Hg^{2+}] and [**L**-Pb^{2+}] systems were insignificant (Fig.8 and Fig.9). It suggested that 3d metal ions could not compete with Hg^{2+} and $Pb^{2+}$to bind with the **L**.

Molecular level interaction

The geometry optimization for **L** was carried out using the hybrid *Ab-initio* (Hartree Fock) method with a 6-311G** basis set as shown in Fig.10. *Ab-initio* (Hartree Fock) method with LANL2DZ effective core potential (ECP) basis set provided a molecular level interaction between **L** and Hg^{2+} as well as **L** and Pb^{2+} have been shown in Fig.11 and Fig.12 respectively. Fig. 13 show the energy gap between highest occupied molecular orbital (HOMO) and lowest unoccupied molecular orbital (LUMO) of the **L**, [**L**-Hg^{2+}] and [**L**-Pb^{2+}] systems. Distinct differential nature of HOMOs and LUMOs of **L** and its metal complexes indicated a molecular level interaction between **L** and these metal ions. Different parameters like, bond moments, dipole moments, quadruple moments along with optimized energies of **L**, [**L**-Hg^{2+}] and [**L**-Pb^{2+}] complexes were presented in the supplementary data (ESI).

IV. APPLICATION

The validity of this newly developed method for trace level determination of Hg^{2+}] and [Pb^{2+}] in environmental samples was checked by analyzing certified reference materials. Solid samples were digested in a microwave oven by the already described analytical procedure. The industrial waste water samples were collected from Damodar river (Durgapur-Raniganj Industrial belt, West Bengal, India) and filtered through 0.45µm Milipore membrane filter followed by its analysis with the proposed chemosensor. The close proximity of the results of analysis of the certified reference materials by the present method clearly indicated its acceptability for the determination of Hg^{2+} and Pb^{2+} in real samples. The results were presented in Table 1 and Table 2 respectively. The observed results are in good agreement with the reported results; no significant differences have been observed (t- test, P = 0.06). The results of the analysis of road dust samples were also included in Table 2.

V. CONCLUSION

New fluorescent probe (**L**) was very efficient for trace level determination of Hg^{2+} and Pb^{2+} ions in aqueous solution. The binding constants of **L** with Hg^{2+} and Pb^{2+} ions were fairly high. FTIR and QTOF-MS ES^+ mass spectra of **L** and its Hg^{2+} and Pb^{2+} complexes clearly indicated the complexation process. Composition of the **L**-Hg^{2+} and **L**-Pb^{2+} complexes in solution were supported by the Job's method. The method was almost free from interferences from 3d metal ions. Finally, computational studies supported the structures and molecular level interactions of **L** with Hg^{2+} and Pb^{2+} ions. The analysis of certified reference materials and real samples were performed to validate this new method.

ACKNOWLEDGEMENT

The authors are grateful to CIPET. Haldia for funding.

APPENDIX A. SUPPLEMENTARY DATA

Electronic Supplementary Information (ESI) is available as a separate file which contains FTIR, ^{1}HNMR and TOF MS spectra of **L** and its Hg^{2+} and Pb^{2+} complexes. It also includes detail results of computational studies.

REFERENCES

[1]. I. Hoyle, and R.D. Handy, (2005), Dose-dependent inorganic mercury absorption by isolated perfused intestine of rainbow trout, *Oncorhynchus mykiss*, involves both amiloride-sensitive and energy-dependent pathways, *quat. Toxicol*. **72**, 147-159.

[2]. A. B. Kobal, M. Horvat, M. Prezelj, A.S. Briˇski, M. Krsnik, T. Dizdareviˇc, D. Mazej,I. Falnoga, V. Stibilj, N. Arneriˇc, and D. Kobal, (2004),The impact of long-term past xposure to elemental mercury on antioxidative capacity and lipid peroxidation in mercury miners, J. Osredkar, *J. Trace Elem. Med. Biol.* **17,** 261-274.

[3]. Z. Marczenko, (1986) *Separation and Spectrophotometric Determination of Elements*, Ellis Horwood, Chichester, pp.15.

[4]. G. Fang, Y. Liu, S. Meng, and Y. Guo, (2002),Spectrophotometric determination of lead in vegetables with dibromo-p-methyl-carboxysulfonazo, *Talanta* **57**,1155-1160.

[5]. J. C. Yu, J. M. Lo, and C.M. Wai, (1983), Extraction of Gold and Mercury from Sea-Water with Bismuth Diethyldithiocarbamate Prior to Neutron-Activation Gamma-Spectrometry, Anal. Chim. Acta. **154**, 307-312.

[6]. P. Ugo, L. M. Moretto, P. Bertoncello, and J. Wang, (1998),Determination of trace mercury in saltwaters at screen-printed electrodes modified with sumichelate Q10R, *Electroanalysis* **10** ,1017-1021.

[7]. L. Bennun, and J. Gomez, (1997), Determination of mercury by total-reflection X-ray fluorescence using amalgamation with gold, *Spectrochim. Acta*, **52B ,**1195-1200.

[8]. M. J. Powell, E. S. K. Quan, D. W. Boomer, and D. R. Wiederin, (1992) ,Inductively coupled plasma mass- spectrometry with direct injection mercury analysis of drinking-water, *Anal.Chem.* **64** ,2233-2237.

[9]. M. S. Bispo, M. G. Andrade Korn, E. S. Bao Morto, and L. S. Gomes Teixeira, (2002), Determination of lead in seawater by inductively coupled plasma optical emission spectrometry after separation and pre-concentration with cocrystallized naphthalene alizarin, *Spectrochim. Acta Part B* **57**, 2175-2180.

[10]. T.-H. Lee, and S.-J. Jiang, (2000), Determination of mercury compounds by capillary electrophoresis inductively coupled plasma mass spectrometry with microconcentric nebulization, *Analytical Chemical Acta*, **413**, 197-205.

[11]. A. D'ulivo, and P. Papoff, (1985), Non-dispersive atomic-fluorescence spectrometric determination of lead by the hydride generation technique, *Talanta* **32 ,** 383-386.

[12]. C. Burrini, and A. Cagnini, (1997), Determination of mercury in urine by ET-ASS and extraction with cyclohexane, *Talanta* **44** ,1219-1223.

[13]. D. L. Tsalev, L. Lampugnani, R. Georgieva, K. K. Chakarova, and I. I. Petrov Jr., (2002), Electrothermal atomic absorption spectrometric determination of cadmium and lead with stabilized phosphate deposited on permanently modified platforms, *Talanta* 58, 331-340.

[14]. A. Shafawi, L. Ebdon, M. Foulkes, P. Stockwell, and W. Corns, (1999), The preliminary evaluation of adsorbent-based mercury removal systems for gas condensate, *Analyst* **124**,185-189.

[15]. Y. Yamini, N. Alizadeh, and M. Shamsipur, (1997), Solid phase extraction and determination of ultra trace amounts of mercury(II) using octadecyl silica membrane disks modified by hexathia-18-crown-6-tetraone and cold vapour atomic absorption spectrometry, *Anal. Chim. Acta*, **355** 69-74.

[16]. Q. W. He, E. W. Miller, A. P. Wong, and C. J. Chang, (2006), A selective fluorescent sensor for detecting lead in living cells, *J. Am. Chem. Soc.* **128** ,9316–9317.

[17]. I. B. Kim, A. Dunkhorst, J. Gilbert, and U. H. F. Bunz, (2005), Sensing of lead ions by a carboxylate-substituted PPE: multivalency, *Macromolecules* **38** ,4560– 4562.

[18]. J. P. Desvergne, and A.W. Czarnik (Eds.), Chemosensors for Ion and Molecule Recognition, Kluwer Academic Publishers, Boston, 1997.

[19]. A.W. Czarnik, (1994), Chemical Communication in Water Using Fluorescent Chemosensors. *Chem. Res.* 27, 302-308.

[20]. B. Vaidya, J. Zak, G.J. Bastiaans, M.D. Porter, J.L. Hallman, N.A.R. Nabulsi, M.D. Ulterback, B. Strzelbicka, and R.A. Bartsch, (1995), Chromogenic and Fluorogenic Crown Ether Compounds for the Selective Extraction and Determination of Hg(II)**,***Anal. Chem*. 67**,** 4101-4111.

[21]. D.Y. Sasaki, and B.E. Padilla, (1998),Dithioamide Metal Ion. Receptors on Fluorescent Lipid Bilayers for the Selective. Optical Detection of Mercuric Ion. *Chem. Commun.***15**, 1581-1582.

[22]. Z. -X. Han, H. -Y. Luo, X. -B.Zhang, R. -M. Kong, G.-L. Shen, and R.-Q. Yu, (2009), A ratiometric chemosensor for fluorescent determination of Hg^{2+} based on a new porphyrin-quinoline dyad, *Spectrochimica Acta Part A* **72**,1084-1088.

[23]. G.G. Talanova, N.S.A. Elkarim, V.S. Talanov, and R.A. Bartsch, (1999) A Calixarene-Based Fluorogenic Reagent for Selective Mercury(II) Recognition. *Anal. Chem.* **71** ,3106-3109.

[24]. Y. -C. Hsieh, J. -L. Chir, H. -H. Wu, P. -S. Chang, and A. -T. Wu, (2009),A sugar-aza-crown ether-based fluorescent sensor for Hg^{2+} and Cu^{2+}, *Carbohydrate Research* **344**, 2236-2239.

[25]. A. Banerjee, D. Karak, A. Sahana, S. Guha, S. Lohar, and D. Das, (2011), Methionine–pyrene hybrid based fluorescent probe for trace level detection and estimation of Hg(II) in aqueous environmental samples: Experimental and computational studies, *J Hazard. Mat.* **186** ,738–744.

[26]. A.W. Czarnik, (1994), Chemical communication in water using fluorescent chemosensor, *Acc. Chem. Res.* **27** ,302-308.

[27]. B. Vaidya, J. Zak, G. J. Bastiaans, M. D. Porter, J. L. Hallman, N. A. R. Nabulsi, M. D. Ulterback, B. Strzelbicka, and R. A. Bartsch, (1995), Chromogenic and Fluorogenic Crown Ether Compounds for the Selective Extraction and Determination of Hg(II), *Anal. Chem.* **67** ,4101-4111.

[28]. D.Y. Sasaki, and B.E. Padilla, (1998), Dithioamide metal ion receptors on Fluorescent lipid bilayers for the selective optical detection of mercuric ion, *Chem. Commun.* **15**, 1581-1582.

[29]. Z. -X. Han, H. -Y. Luo, X. -B.Zhang, R. -M. Kong, G. -L. Shen, and R. -Q. Yu, (2009), A ratiometric chemosensor for fluorescent determination of Hg^{2+} based on a new porphyrin-quinoline dyad, *Spectrochimica Acta Part A* **72**,1084–1088.

[30]. G. G. Talanova, N. S. A. Elkarim, V. S. Talanov, and R.A. Bartsch, (1999), A calixarene based fluorogenic reagent for selective mercury (II) recognition, *Anal. Chem.* **71**,3106-3109.

[31]. Y. -C. Hsieh, J. -L. Chir, H. -H. Wu, P. -S. Chang, and A. -T. Wu, (2009), A sugar-aza-crown ether-based fluorescent sensor for Hg^{2+} and Cu^{2+}, *Carbohyd. Res.* **344**, 2236–2239.

[32]. V. Camel, (2003), Solid phase extraction of trace elements, Spectrochim. Acta, Part B **58** 1177-1233.

[33]. R. A. Goyer, (1986) *In Casarett and Doull's Toxicology: The basic science of poisons*; C.D. Klaassen, M.O. Amdur, J. Doull, Eds.; 3rd ed. Mac Millan publisher: New York, pp 598.

[34]. R. Métivier, I. Leray, and B. Valeur, (2003) A highly sensitive and selective fluorescent molecular sensor for Pb(II) based on a calix[4]arene bearing four dansyl groups, *Chem. Commun.***8**, 996 - 997.

[35]. F. Y. Wu, S. W. Bae, and J. I. Hong, (2006), A selective fluorescent sensor for Pb(II) in water, *Tetrahedron Lett*. **47**, 8851-8854.

[36]. M. Arduini, F. Mancin, P. Tecilla, and U. Tonellato, (2007),Self-organized fluorescent nanosensors for ratiometric Pb^{2+} detection, *Langmuir* **23,**8632- 8636.

[37]. S. S. Bozkurt, S. Ayata, and I. Kaynak, (2009), Fluorescence-based sensor for Pb(II) using tetra-(3-bromo-4-hydroxyphenyl)porphyrin in liquid and immobilized medium, *Spectrochim. Acta A* **72**, 880-883.

[38]. L. Ma, Y. Li, L. Li, Y. Wu, R. Buchet, and Y. Ding, (2009),Clarification of the binding model of lead(II) with a highly sensitive and selective fluoroionophore sensor by spectroscopic and structural study, *Spectrochim. Acta A* **72** ,306-311.

[39]. X. L. Ni, S. Wang, X. Zeng, Z. Tao, and T. Yamato, (2011)**,** Pyrene-Linked Triazole-Modified Homooxacalix[3]arene: A Unique C3 Symmetry Ratiometric Fluorescent Chemosensor for Pb^{2+}, *Org. Lett.* **13,** 552 -555.

[40]. S. Goswami, and R. Chakrabarty, (2010), Highly Selective Colorimetric Fluorescent Sensor for Pb^{2+},*Eur. J. Org. Chem.***2010**(20),3791-3795.

[41]. T. Lan, K. Furuya, and Y. Lu, (2010), A highly selective lead sensor based on a classic lead DNAzyme, *Chem. Commun.* **46**, 3896- 3898.

[42]. H. Ju, M. H. Lee, J. Kim, J. S. Kim, and J. Kim, (2011), Rhodamine-based chemosensing monolayers on glass as a facile fluorescent "turn-on" sensing film for selective of Pb^{2+} , *Talanta* **83**, 1359- 1363.

[43]. U. P. Masche, K. M. Rentsch, Avon Felten, P. J. Meier, and K. E. Fittinger, (1999), No clinically relevant effect of Iornoxicam intake on acenocoumarol pharmacokinetics and pharmacodynamics, *Eur. J. Clin. Pharmacol.* **5**, 865-868.

[44]. I. P. Kostova, I. Manolov, I. Nikolova, and N. Danchev, (2001),New metal complexes of 4- methyl-7-hyd.roxycouma.rin sodium salt and their pharmacological activity. *Farmaco* **56** ,707-713.

[45]. F. A. Jimenez-Orozco, J. A. Molina-Guarneros, N. Mendoza-Patino, F. Leon-Cedeno, B. Flores-Perez, E. Santos-Santos, and J. J. Mandoki, (1999), Cytostatic activity of coumarin metabolites and derivatives in the B16-F10 murine melanoma cell line. *Melanoma Res.* **9**(3),243-248.

[46]. G. J. Finn, B. S. Creaven, and D. A. Egan, (2001),Study of the in vitro cytotoxic potential of natural and synthetic coumarin derivatives using human normal and neoplastic skin cell lines, Melanoma Res. **11**,461-467.

[47]. P. Laurin, M. Klich, C. Dupis-Hamelin, P. Mauvais, P. Lassaigne, A. Bonnefoy, and B. Musicki, (1999), Synthesis and in vitro evaluation of novel highly potent coumarin inhibitors of gyrase, *Bioorg. Med. Chem. Lett.* **9**,2079-2084.

[48]. R. J. S. Hoult, and M. Paya, (1996), Pharmacological and biochemical actions of simple coumarins: natural products with therapeutic potential, *Gen. Pharmacol.* **27**, 713-722.

[49]. S. P. Pillai, S. R. Menon, L. A. Mitscher, C. A. Pillai, and D. A. Shankel, (1999), Umbelliferone Analogues and Their Potential to Inhibit Benzo(a)pyrene and Hydrogen Peroxide Induced Mutations. *J. Nat. Prod.* **62,** 1358-1360.

[50]. Y. Kimura, H. Okuda, S. Arichi, K. Baba, and M. Kozawa, (1985), Inhibition of the formation of 5-hydroxy-6,8,11,14-eicosatetraenoic acid from arachidonic acid, *Biochim. Biophys. Acta*, **834**,224-229.

[51]. J. Hoffmanova, A. Kozubik, and L. Dusek, (1998), Inhibitors of lipoxygenase metabolism exert synergistic effects with retinoic acid on differentiation of human leukemia HL-60 cells J. Pachernik, *Eur. J. Pharmacol*. **350**, 273-284.

[52]. G. J. Finn, B. S. Creaven, and D. A. Egan, (2004), A study of the role of cell cycle events mediating the action of coumarin derivatives in human malignant melanoma cells, *Cancer Lett.* **214** ,43-54.

[53]. G. J. Finn, B. S. Creaven, and D.A. Egan, (2005), Activation of mitogen activated protein kinase pathways and melanogenesis by novel nitro-derivatives of 7-hydroxycomarin in human malignant melanoma cells, *Eur. J. Pharm. Sci.* **26**,16-25.

[54]. Gaussian 03, Rev.C.02, Gaussian Inc., Wallingford CT, 2004.

Legends to Figures

Scheme1. Synthesis of the fluorescent probe (6E)-6-((2-hydroxynaphthalen-3-yl)methyleneamino)-2H-chromen-2-one (**L**) selective for Hg^{2+} and Pb^{2+}.

Scheme2. **L** binds with Hg^{2+}ion and Pb^{2+} ion.

Fig. 1. Changes in the fluorescence emission intensities of (**L**) upon gradual addition of Hg^{2+} ion. Inset plot shows the emission intensities of [L] (10 μM) as a function of externally added [Hg^{2+}] (λ_{ex} = 253 nm, λ_{em} = 350 nm, [**L**] = 10^{-6} mol L^{-1}, methanol: water = 4:1, v/v).

Fig. 2. Changes in the fluorescence emission intensities of (**L**) upon gradual addition of Pb^{2+} ion. Inset plot shows the emission intensities of [L] (10 μM) as a function of externally added [Pb^{2+}] (λ_{ex} = 253 nm, λ_{em} = 350 nm, [**L**] = 10^{-6} mol L^{-1}, methanol: water = 4:1, v/v).

Fig. 3. Job's plots for the determinations of the stoichiometry of the complexes formed between **L** and Hg^{2+} in solution.

Fig. 4. Job's plots for the determinations of the stoichiometry of the complexes formed between **L** and Pb^{2+} in solution.

Fig. 5. Determinations of binding constants of **L** with Hg^{2+} ions using Benesi- Hildebrand equation.

Fig. 6. Determinations of binding constants of **L** with Pb^{2+} ions using Benesi- Hildebrand equation.

Fig.7 . Effect of different metal ions (M^{n+}) on the emission intensity of **L** (λ_{ex} = 253 nm, λ_{em} = 350 nm, [L] = [M^{n+}] = 1 μM, methanol: water = 4:1, v/v).

Fig. 8. Studies on interferences from 3d metal ions on the emission intensity of the [**L**-Hg^{2+}] systems. ([**L**] = 10 μM; [Hg^{2+}] = [M^{n+}]). Inset plot shows pink bars represent emission intensity of **L** with Hg^{2+} ions whereas blue bars show the intensities of the [**L**-Hg^{2+}] systems upon addition of foreign metal ion. Red bars represent the extent of interferences.

Fig. 9. Studies on interferences from 3d metal ions on the emission intensity of the [**L**-Pb^{2+}] systems. ([**L**] = 10 μM; [Pb^{2+}] = [M^{n+}]). Inset plot shows pink bars represent emission intensity of **L** with Pb^{2+} ions whereas blue bars show the intensities of the [**L**-Pb^{2+}] systems upon addition of foreign metal ion. Red bars represent the extent of interferences.

Fig. 10. Stereoscopic view of the energy optimized geometry of **L** with *Ab-initio*, Hartree Fock) method using 6-311G* basis set.

Figure 8. Stereoscopic view of the energy optimized geometry of [**L** - Hg^{2+}] complex with *Ab-initio*, Hartree Fock) method.

Figure 9. Stereoscopic view of the energy optimized geometry of [**L** - Pb^{2+}] complex with *Ab-initio*, Hartree Fock) method.

Figure10. HOMO- LUMO pictures of **L**, [**L**-Hg^{2+}] and [**L**+Pb^{2+}] systems.

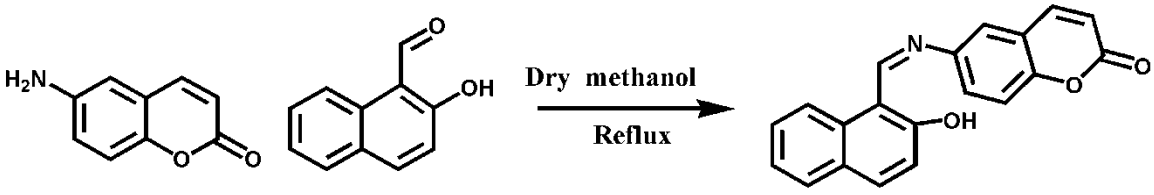

(6*Z*)-6-((2-hydroxynaphthalen-1-yl)methyleneamino)-2*H*-chromen-2-one

Scheme1

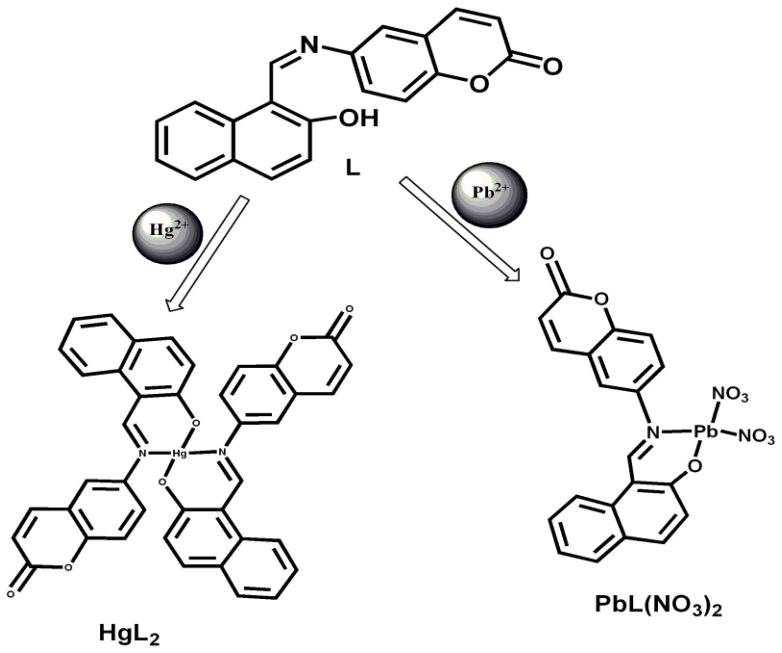

Scheme 2

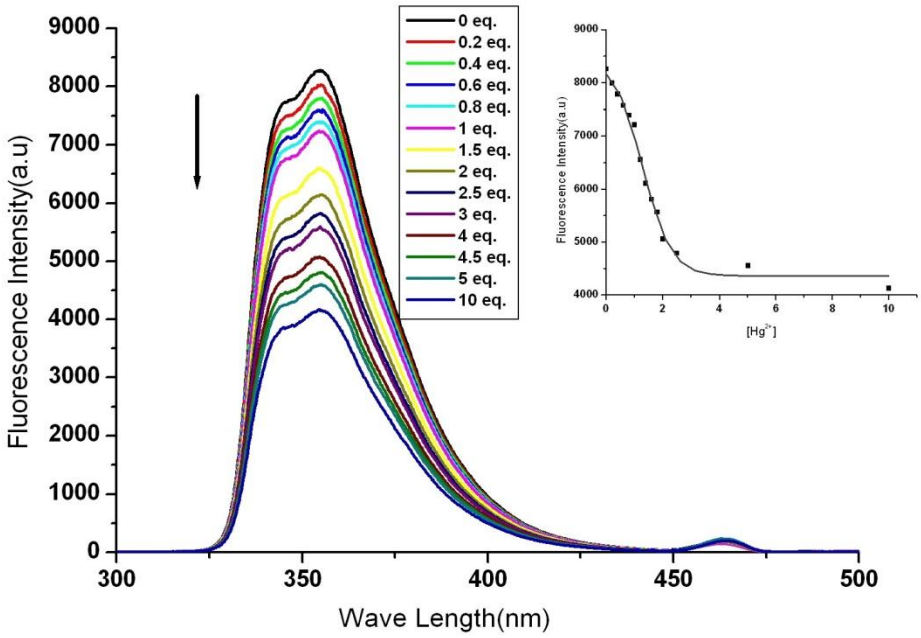

Fig.1

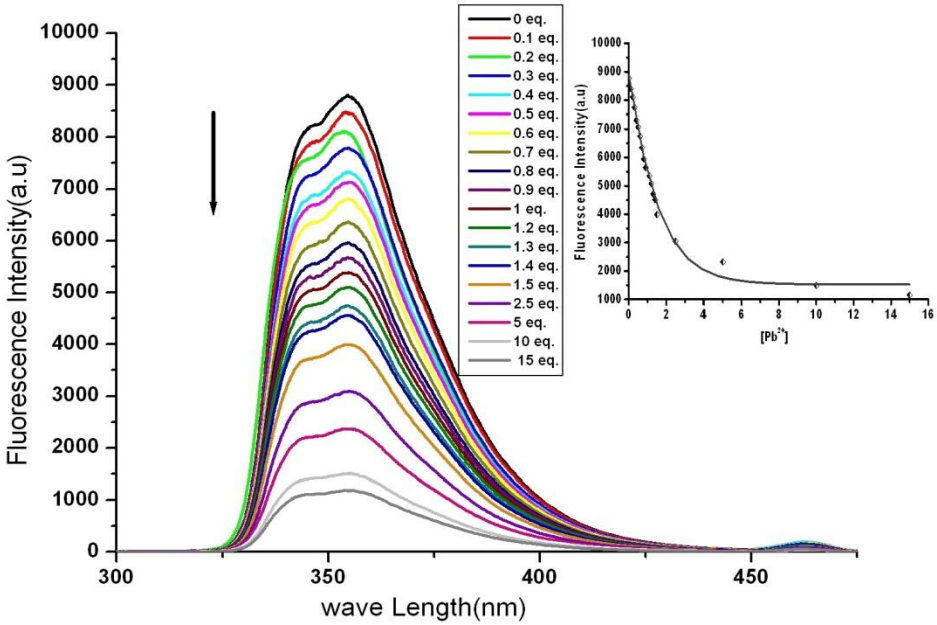
Fluorescence Intensity(a.u)
wave Length(nm)
0 eq.
0.1 eq.
0.2 eq.
0.3 eq.
0.4 eq.
0.5 eq.
0.6 eq.
0.7 eq.
0.8 eq.
0.9 eq.
1 eq.
1.2 eq.
1.3 eq.
1.4 eq.
1.5 eq.
2.5 eq.
5 eq.
10 eq.
15 eq.
Fluorescence Intensity(a.u)
[Pb2+]

Fig.2

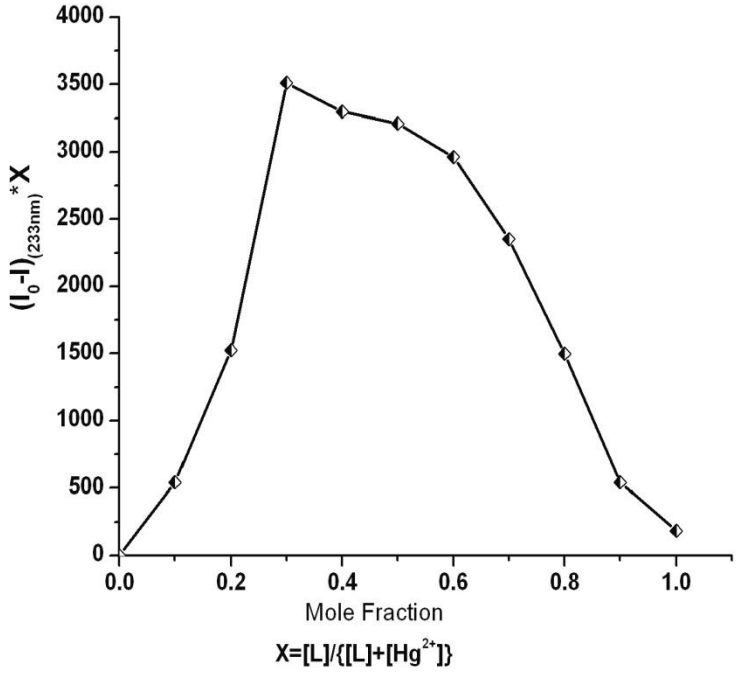
(I0-I)(233nm) *X
Mole Fraction
X=[L]/{[L]+[Hg2+]}

Fig.3

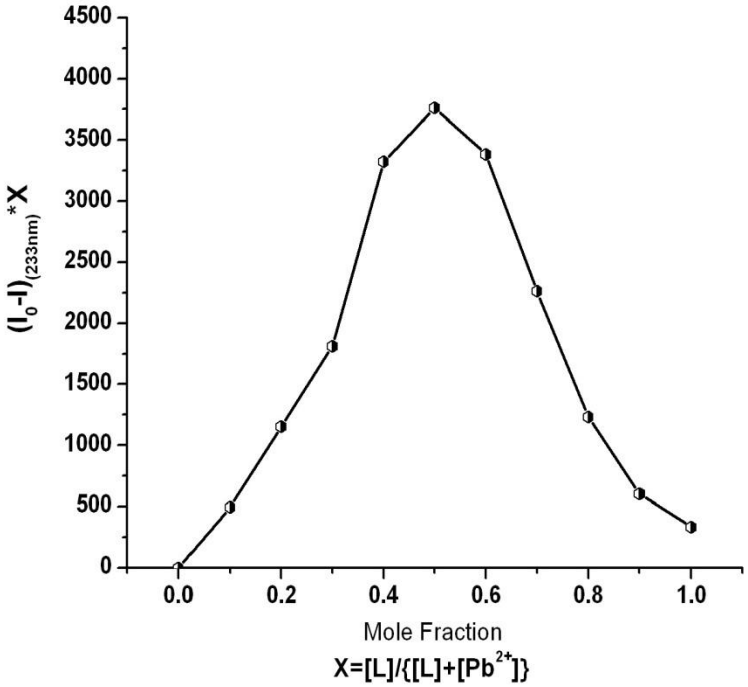
4500
4000
3500
3000
2500
2000
1500
1000
500
0
0.0
0.2
0.4
0.6
0.8
1.0
$(I_0-I)_{(233nm)}$ *X
Mole Fraction
X=[L]/{[L]+[Pb^{2+}]}

Fig.4

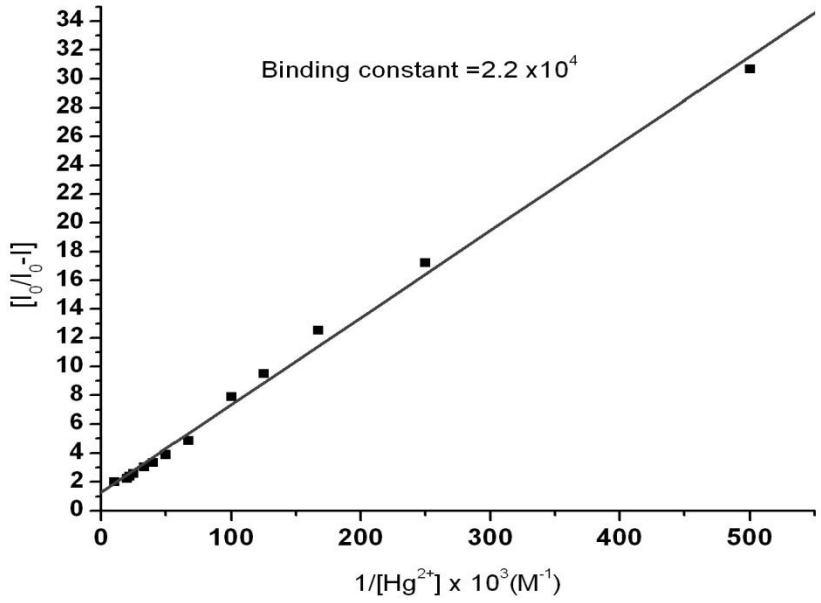
Binding constant =2.2 x10^4
$[I_0/I_0-I]$
0
2
4
6
8
10
12
14
16
18
20
22
24
26
28
30
32
34
0
100
200
300
400
500
1/[Hg^{2+}] x 10^3(M^{-1})

Fig.5

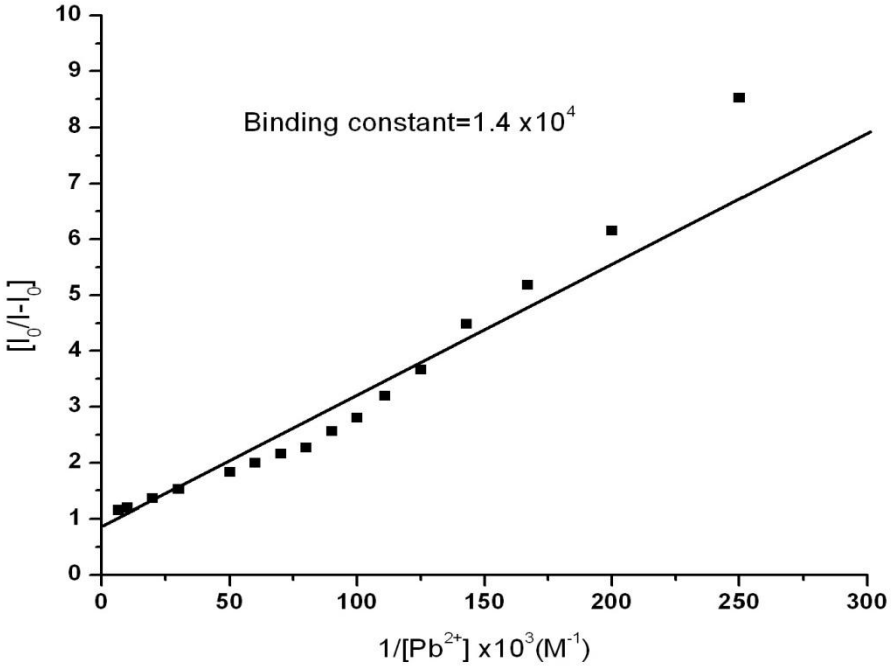
Binding constant=1.4 x10^4
[I0/I-I0]
1/[Pb2+] x10^3(M-1)
0
1
2
3
4
5
6
7
8
9
10
0
50
100
150
200
250
300

Fig.6

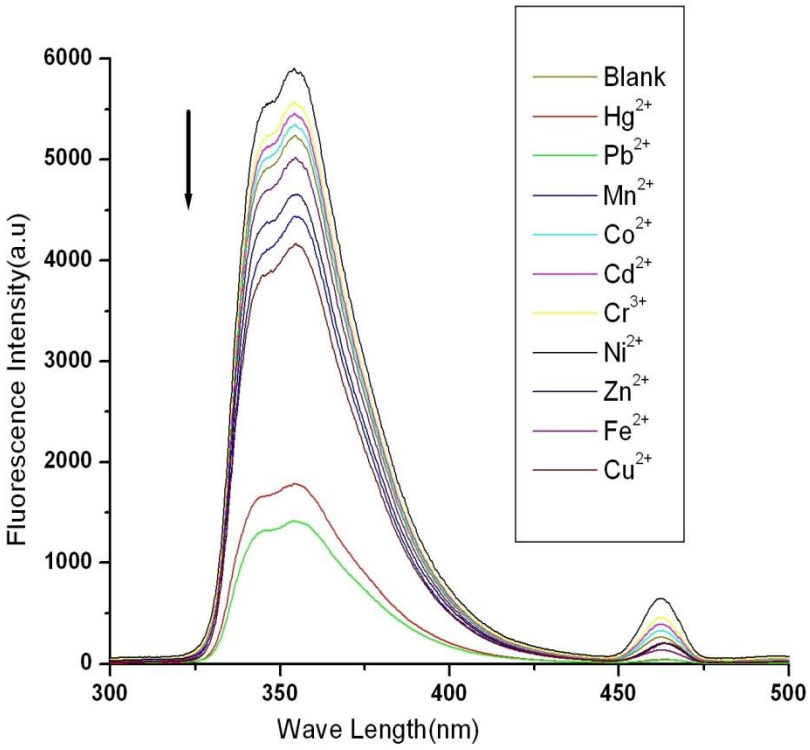
Blank
Hg2+
Pb2+
Mn2+
Co2+
Cd2+
Cr3+
Ni2+
Zn2+
Fe2+
Cu2+
Fluorescence Intensity(a.u)
Wave Length(nm)
0
1000
2000
3000
4000
5000
6000
300
350
400
450
500

Fig.7

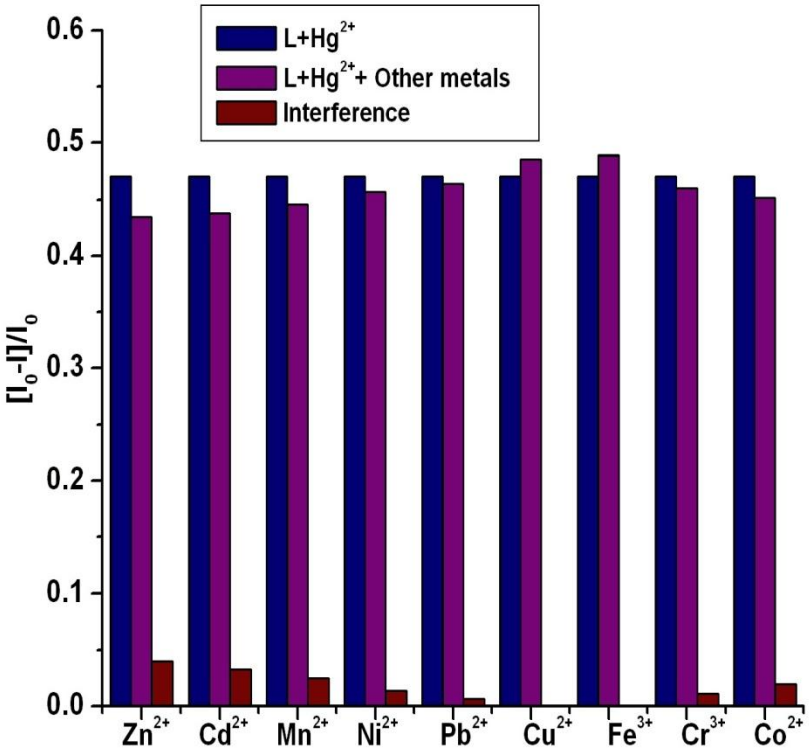
L+Hg2+
L+Hg2++ Other metals
Interference
[I0-I]/I0
0.0
0.1
0.2
0.3
0.4
0.5
0.6
Zn2+
Cd2+
Mn2+
Ni2+
Pb2+
Cu2+
Fe3+
Cr3+
Co2+

Fig.8

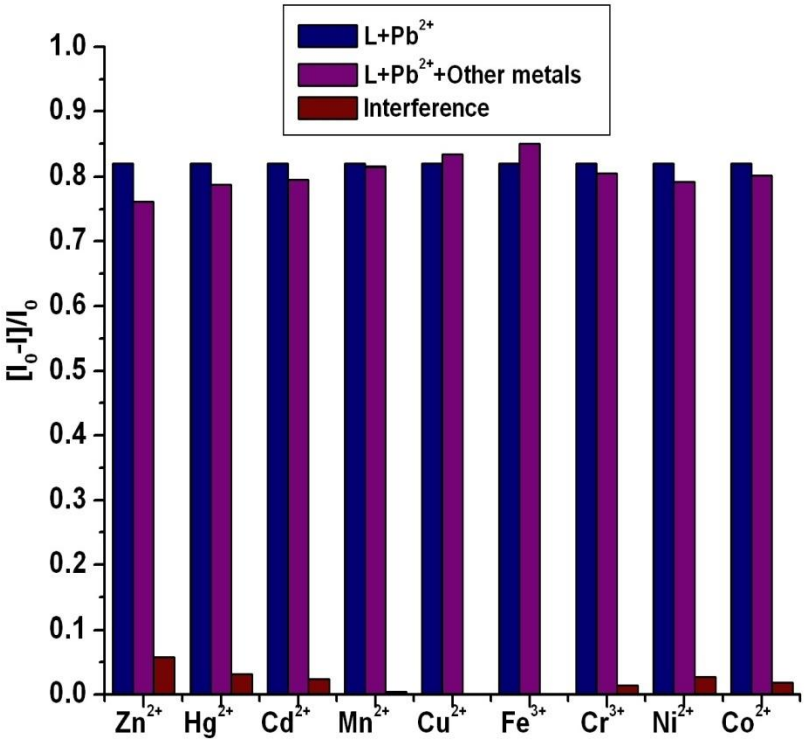
L+Pb2+
L+Pb2++Other metals
Interference
[I0-I]/I0
0.0
0.1
0.2
0.3
0.4
0.5
0.6
0.7
0.8
0.9
1.0
Zn2+
Hg2+
Cd2+
Mn2+
Cu2+
Fe3+
Cr3+
Ni2+
Co2+

Fig.9

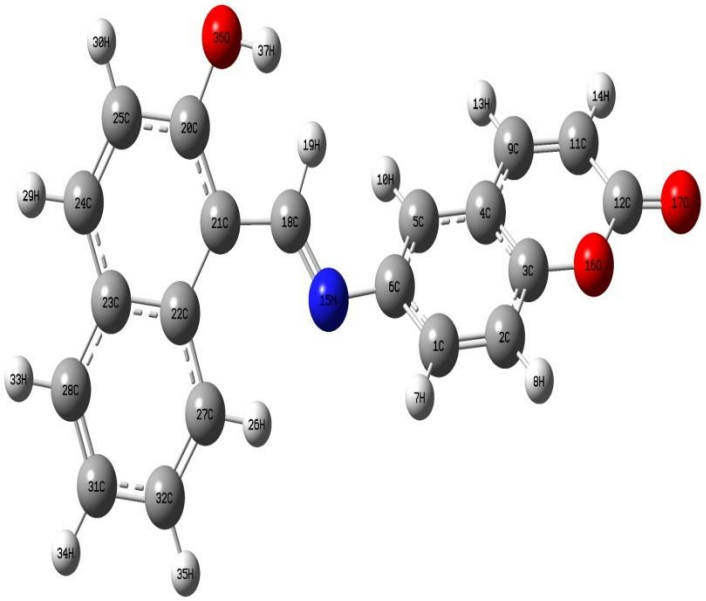
38H
37H
25C
20C
19H
13H
14H
9C
11C
29H
24C
21C
18C
10H
5C
4C
12C
17O
23C
22C
15N
6C
3C
16O
1C
2C
33H
28C
27C
26H
7H
8H
31C
32C
34H
35H

Fig.10

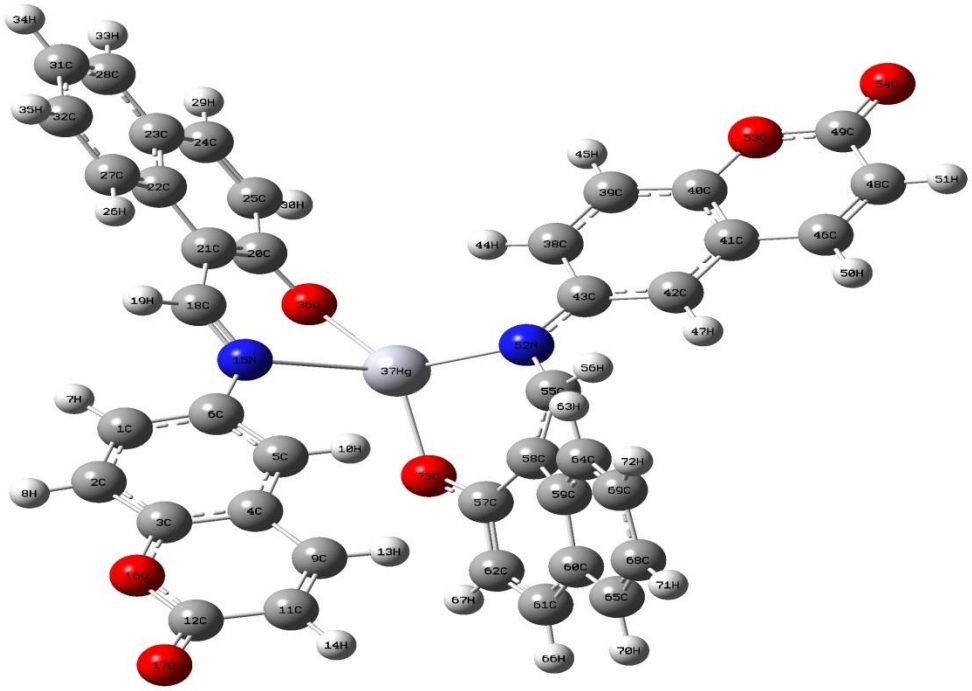
34H
33H
31C
28C
29H
35H
32C
23C
24C
27C
22C
25C
30H
26H
21C
20C
19H
18C
30O
15N
37Hg
52N
56H
55C
63H
7H
1C
6C
5C
10H
58C
64C
72H
8H
2C
30O
57C
59C
69C
3C
4C
9C
13H
16O
62C
60C
68C
71H
67H
61C
55C
12C
11C
14H
17O
66H
70H
54O
49C
53O
45H
39C
40C
48C
51H
44H
38C
41C
46C
50H
43C
42C
47H

Fig.11

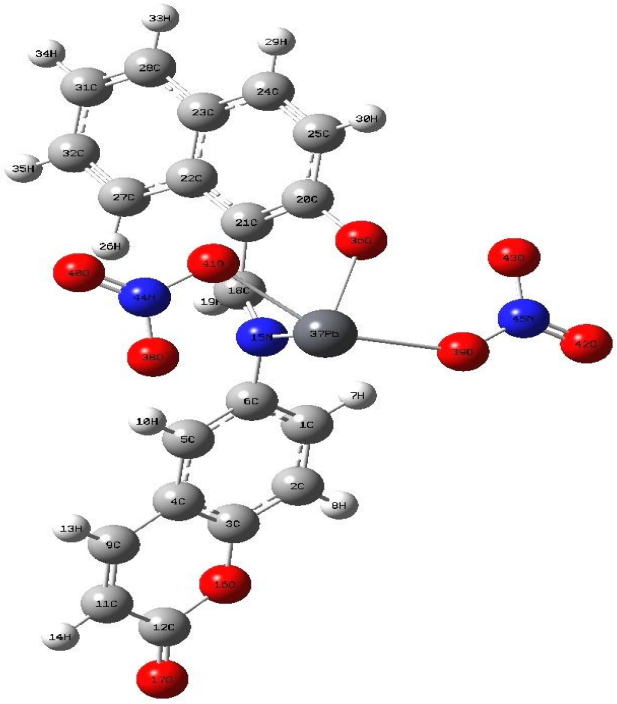
33H
29H
34H
28C
31C
24C
23C
25C
30H
32C
35H
22C
27C
20C
21C
26H
19C
18C
37Pb
6C
7H
10H
5C
1C
2C
4C
8H
3C
13H
9C
11C
12C
14H

Fig.12

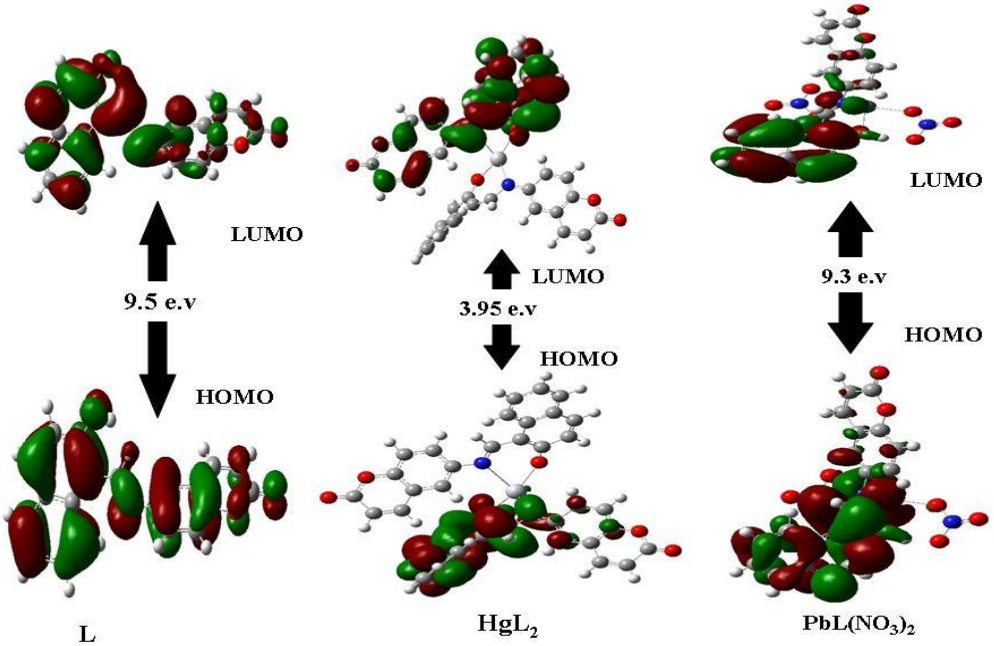
LUMO
9.5 e.v
HOMO
L
LUMO
3.95 e.v
HOMO
HgL2
LUMO
9.3 e.v
HOMO
PbL(NO3)2

Fig.13

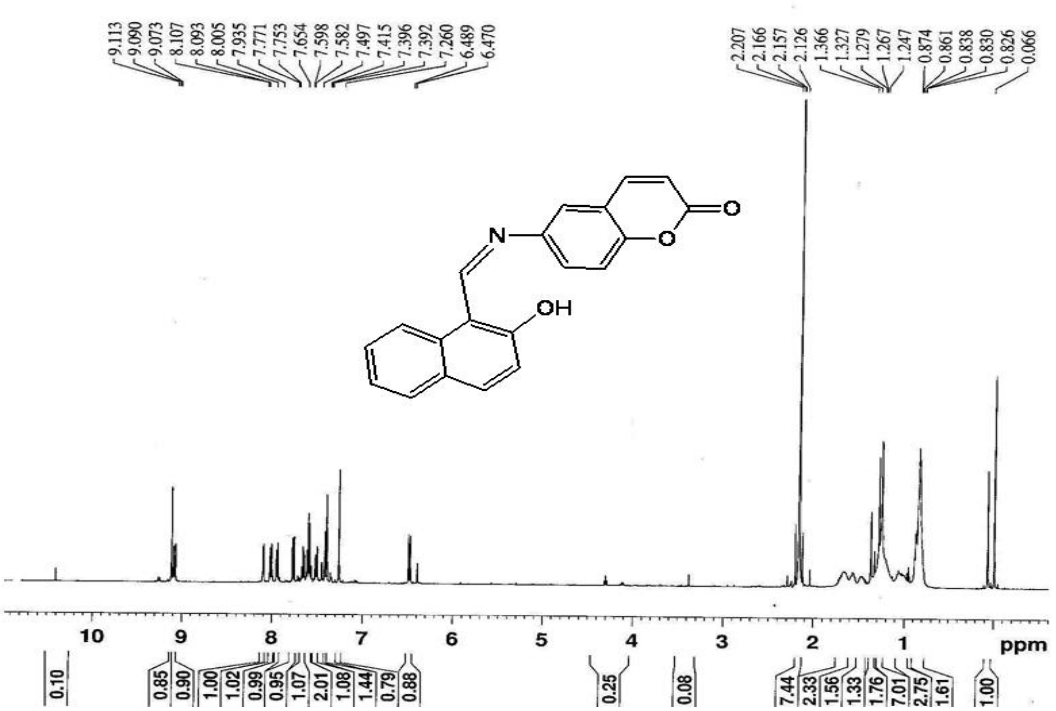

S1. ^{1}H-NMR spectra of L

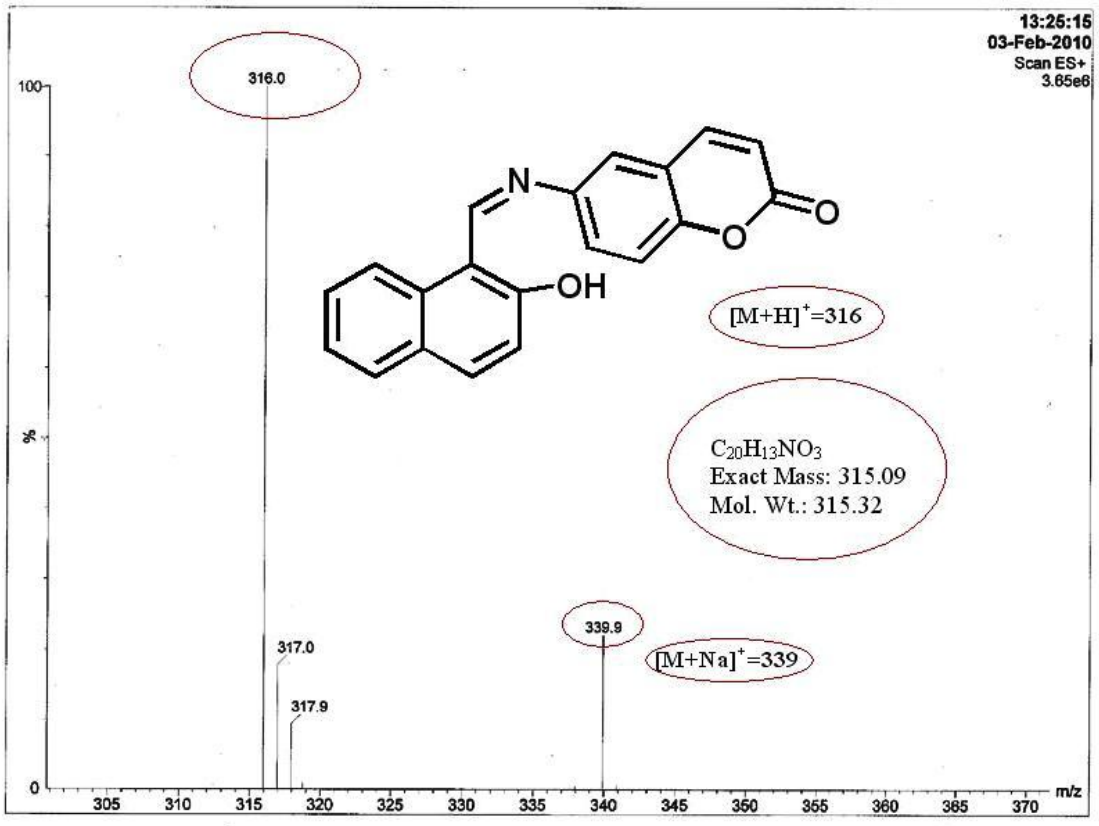

S2. TOF MS ES (+) mass spectra of L

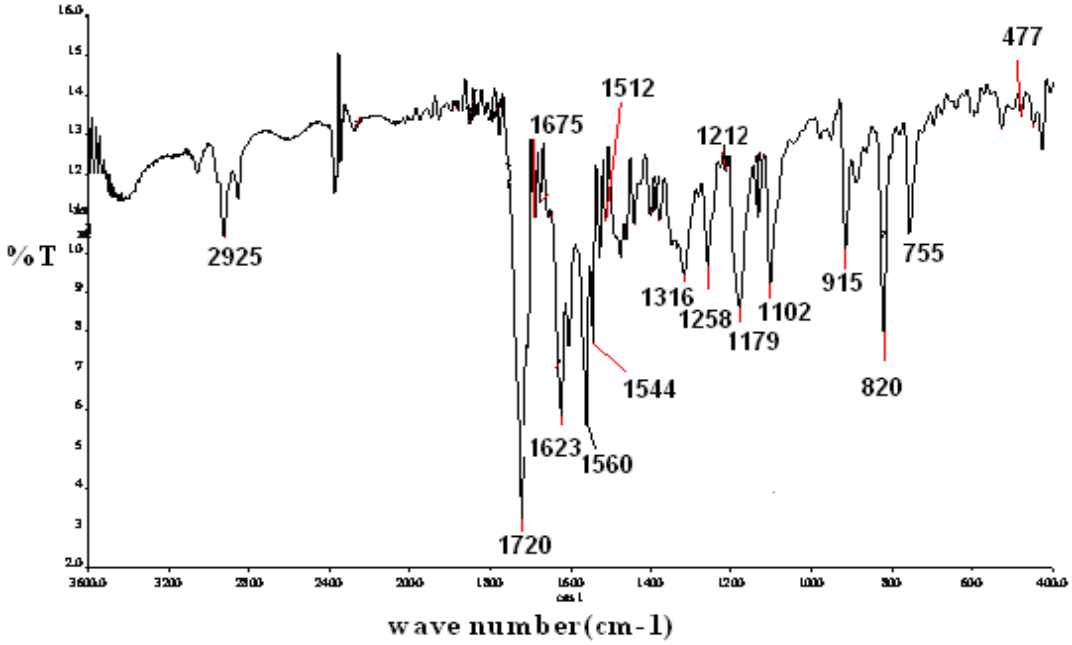

S3. FTIR spectra of L

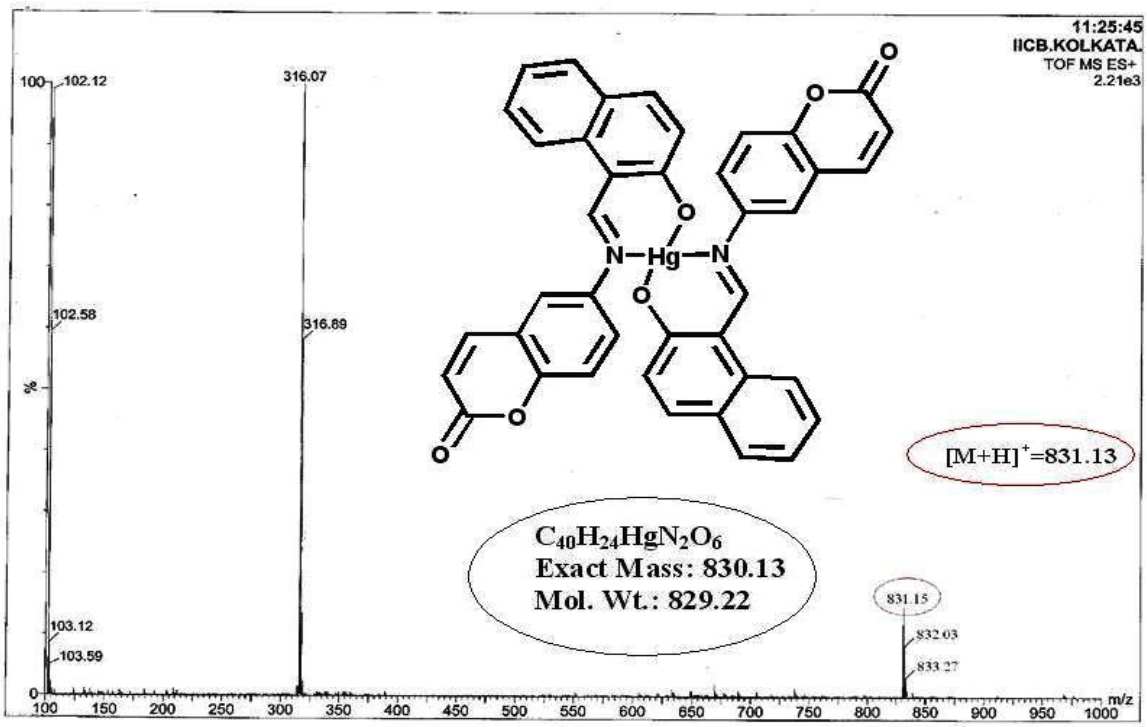

S4. TOF MS ES (+) mass spectra of L+Hg^{2+}

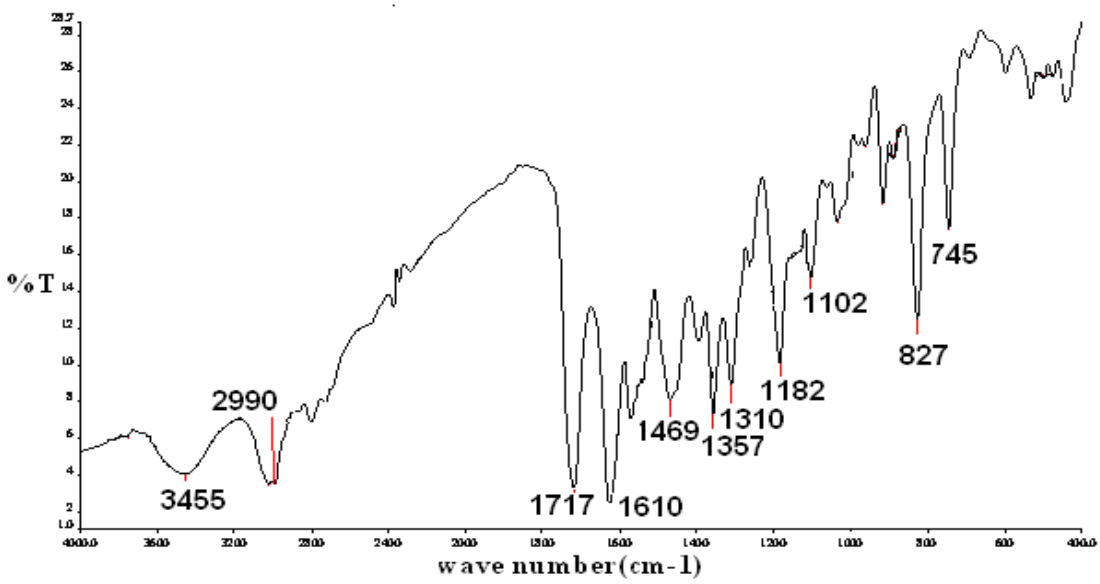

S5. FTIR spectra of the L- Hg^{2+} complex

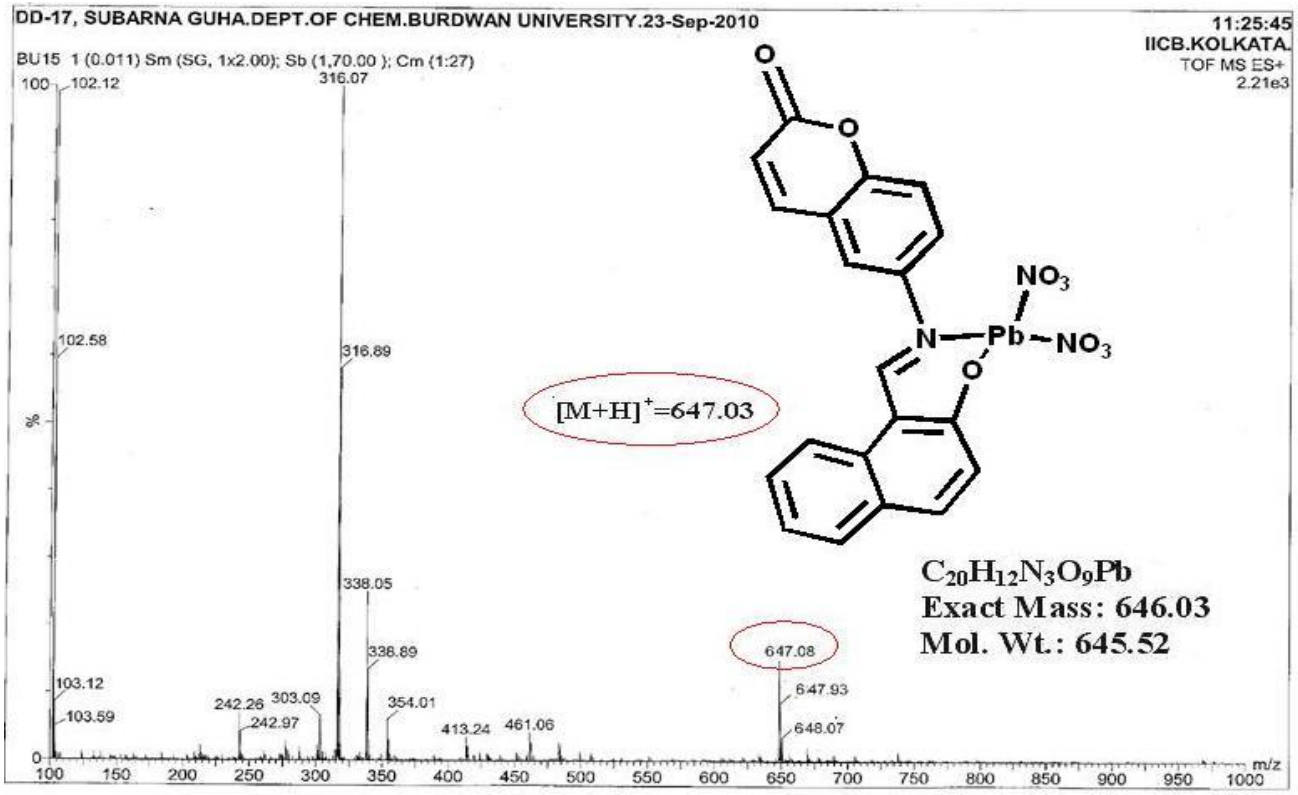

S6. TOF MS ES (+) mass spectra of $L+Pb^{2+}$

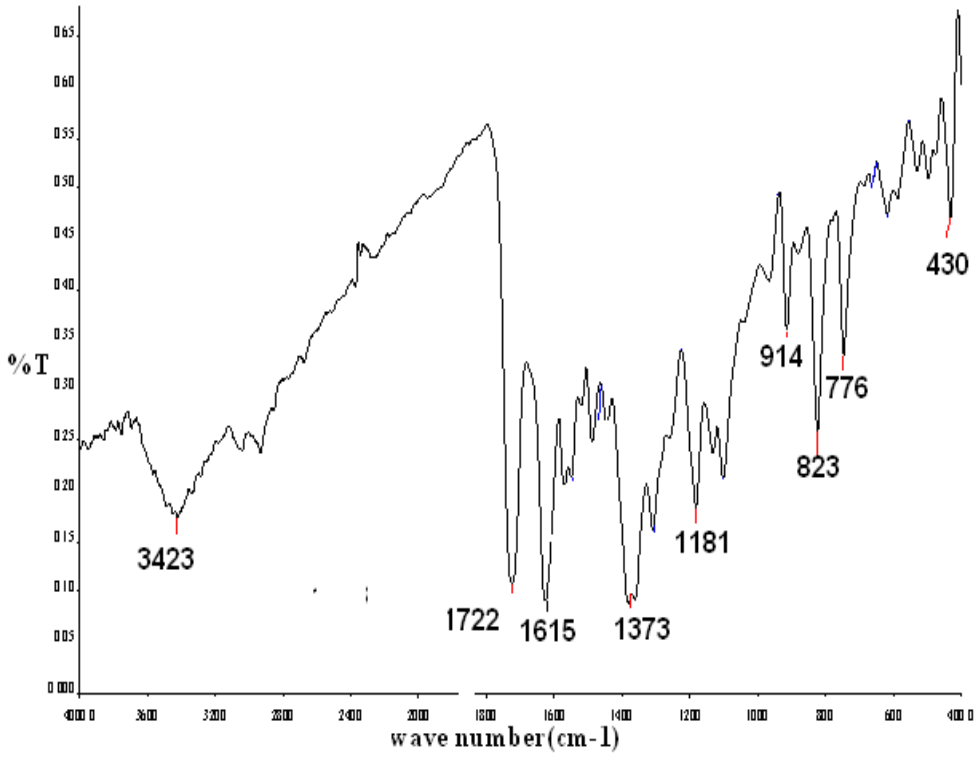

S7. FTIR spectra of the L- Pb^{2+}complex

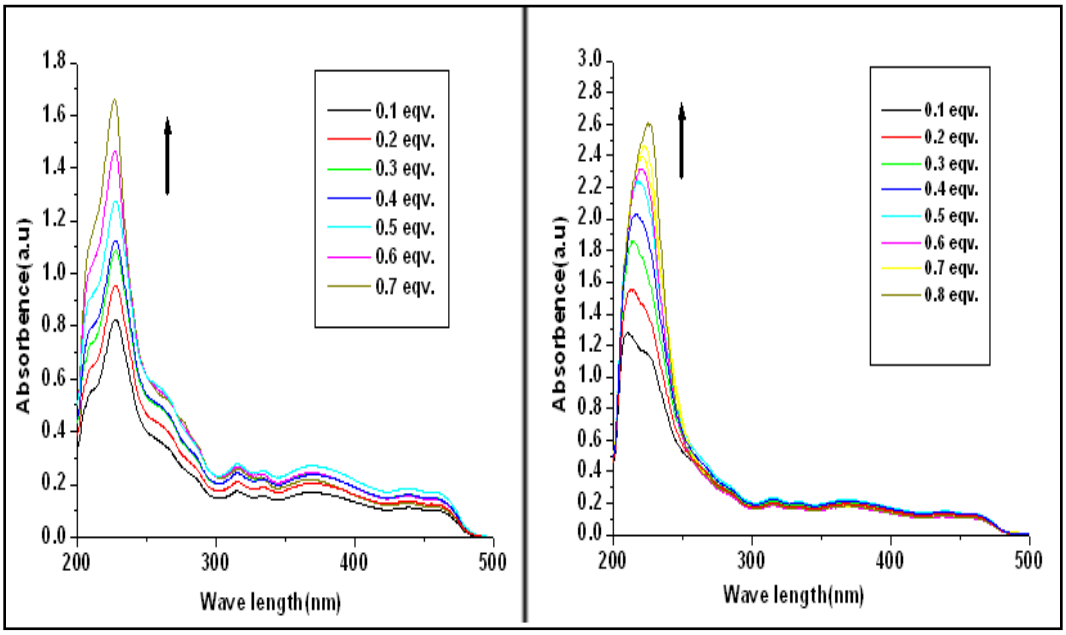

S8. UV-Vis titration spectra of the L- Hg^{2+} and L- Pb^{2+} complex in methanol ([L] = 10^{-4} $molL^{-1}$; [Complex] = 10^{-4} mol L^{-1})

S9. Various bond lengths, angles and dihedral angles of L generated by *Ab-initio*, Hartree Fock method potential in conjuration with a 6-311G* basis set method

Row	Highlight	Tag	Symbol	NA	NB	NC	Bond	Angle	Dihedral	X	Y	Z
1	No	1	C							1.7860700	-1.0066950	1.5590360
2	No	2	C	1			1.3741301			3.1595130	-1.0305970	1.5953190
3	No	3	C	2	1		1.3868084	119.2560223		3.8750760	-0.4538910	0.5567540
4	No	4	C	3	2	1	1.3821023	120.8326056	-0.2355725	3.2239940	0.1365340	-0.5098750
5	No	5	C	4	3	2	1.3963058	119.2451409	0.8852543	1.8280720	0.1650700	-0.5259150
6	No	6	C	5	4	3	1.3800825	120.6795909	0.1237970	1.1005520	-0.3858180	0.5093940
7	No	7	H	1	2	3	1.0741538	120.3659164	179.0787991	1.2140800	-1.4609960	2.3465920
8	No	8	H	2	1	6	1.0735967	121.5805465	179.1705334	3.6926110	-1.4936040	2.4040470
9	No	9	C	4	3	2	1.4530436	117.0909882	-178.5331174	4.0530240	0.6867980	-1.5687680
10	No	10	H	5	4	3	1.0752493	119.0153091	-177.9587819	1.3249220	0.5956440	-1.3730320
11	No	11	C	9	4	3	1.3280977	120.3829867	-0.6465162	5.3770950	0.6247630	-1.4861180
12	No	12	C	11	9	4	1.4694243	121.1663063	0.1141573	6.0385840	0.0006420	-0.3319460
13	No	13	H	9	4	3	1.0758948	118.8605580	179.4142268	3.5755640	1.1445730	-2.4173100
14	No	14	H	11	9	4	1.0721414	123.2522196	-179.9213055	6.0321210	1.0165370	-2.2390730
15	No	15	N	6	5	4	1.4076906	123.6157499	-179.0663877	-0.3064410	-0.4082600	0.5476010
16	No	16	O	12	11	9	1.3510391	116.2179265	0.3998628	5.2250120	-0.5055280	0.6205240
17	No	17	O	12	11	9	1.1775349	124.7146976	-179.6475095	7.2047500	-0.0831210	-0.1918420
18	No	18	C	15	6	5	1.2552900	119.5090189	-44.4655775	-0.9499940	0.6231880	0.2350190
19	No	19	H	18	15	6	1.0864975	119.5897637	-2.5938513	-0.4140260	1.5331540	-0.0202790
20	No	20	C	18	15	6	2.4284991	152.0868279	-157.3884334	-2.9417530	2.0111910	0.2978820
21	No	21	C	20	18	15	1.3725599	32.8256683	-42.8685629	-2.4197100	0.7479540	0.1728860
22	No	22	C	21	20	18	1.4450008	118.6332084	-176.7714570	-3.3218730	-0.3522910	-0.0792850
23	No	23	C	22	21	20	1.4091420	118.9486101	2.0572028	-4.6971410	-0.0855230	-0.2314490
24	No	24	C	23	22	21	1.4213987	119.5392914	-0.7532161	-5.1685030	1.2506680	-0.1183750
25	No	25	C	24	23	22	1.3489213	121.1695044	-0.5377760	-4.3236840	2.2692500	0.1430830
26	No	26	H	22	21	20	2.1536913	97.8792650	-178.2899949	-1.8619010	-1.9355850	-0.0862050
27	No	27	C	22	21	20	1.4194813	123.4950177	-179.1997131	-2.8962930	-1.7001740	-0.2097470
28	No	28	C	23	22	21	1.4153850	120.2013835	179.0525091	-5.6017360	-1.1406910	-0.4991110
29	No	29	H	24	23	22	1.0756523	118.7877078	-179.8770795	-6.2209020	1.4402900	-0.2346840
30	No	30	H	25	24	23	1.0734125	122.2935967	-178.9219242	-4.6622550	3.2823510	0.2489620
31	No	31	C	28	23	22	1.3576750	120.8863769	-0.2015933	-5.1643210	-2.4204990	-0.6176060
32	No	32	C	27	22	21	1.3618773	120.9159444	-178.8242541	-3.7900640	-2.6939530	-0.4710640
33	No	33	H	28	23	22	1.0759514	118.5750017	179.9020179	-6.6463810	-0.9075930	-0.6089000
34	No	34	H	31	28	23	1.0749941	120.6598217	179.9850467	-5.8546140	-3.2191590	-0.8207070
35	No	35	H	32	27	22	1.0756163	119.2955614	-	-	-	-0.5635130

									179.9227681	3.4391510	3.7065060	
36	No	36	O	20	18	15	1.3536339	91.0918749	133.2837656	-2.1982700	3.1112780	0.5612570
37	No	37	H	36	20	18	0.9393039	112.0770093	-33.9550615	-1.4483840	2.9121290	1.0906930

S10. Physical parameters of the ligand L

Sum of Mulliken charges= 0.00000

Electronic spatial extent (au): <R**2>= 11522.7781

Charge= 0.0000 electrons

Dipole moment (field-independent basis, Debye):

X= -5.3877 Y= 1.3917 Z= -1.0861 Tot= 5.6696

Quadrupole moment (field-independent basis, Debye-Ang):

XX= -172.2051 YY= -133.4012 ZZ= -133.3438

XY= 5.7433 XZ= -5.1427 YZ= -1.1320

Traceless Quadrupole moment (field-independent basis, Debye-Ang):

XX= -25.8884 YY= 12.9155 ZZ= 12.9729

XY= 5.7433 XZ= -5.1427 YZ= -1.1320

Octapole moment (field-independent basis, Debye-Ang**2):

XXX= -515.2418 YYY= -18.6201 ZZZ= 9.1754 XYY= 0.2352

XXY= 34.4413 XXZ= -54.9456 XZZ= 58.8102 YZZ= 10.1631

YYZ= 4.6626 XYZ= -23.4359

Hexadecapole moment (field-independent basis, Debye-Ang**3):

XXXX=-15866.0002 YYYY= -1710.6745 ZZZZ= -626.0883 XXXY= 125.0828

XXXZ= -100.9694 YYYX= 55.4335 YYYZ= 37.8112 ZZZX= -40.1295

ZZZY= -36.8867 XXYY= -2362.9414 XXZZ= -2314.7625 YYZZ= -386.2933

XXYZ= -19.5718 YYXZ= 24.8031 ZZXY= -13.8432

N-N= 1.784461753962D+03 E-N=-6.010395012924D+03 KE= 1.044201261066D+03

S11. Various bond lengths, angles and dihedral angles of L +Hg^{2+} generated by HF method

Row	Highlight	Tag	Symbol	NA	NB	NC	Bond	Angle	Dihedral	X	Y	Z
1	No	1	C							-3.3926110	3.0468600	0.0512420
2	No	2	C	1			1.3905450			-4.7478790	2.8028840	0.2444770
3	No	3	C	2	1		1.3848945	118.8015069		-5.1756490	1.4941340	0.3932020
4	No	4	C	3	2	1	1.3950352	121.4164489	-0.9590839	-4.2810250	0.4254160	0.3330940
5	No	5	C	4	3	2	1.3971119	119.1165629	1.6943472	-2.9203990	0.6870900	0.1538030
6	No	6	C	5	4	3	1.3924634	120.6952276	-0.1506811	-2.4579800	1.9949560	0.0329330
7	No	7	H	1	2	3	1.0719536	118.7281115	176.5051918	-3.0698320	4.0545590	-0.1203420
8	No	8	H	2	1	6	1.0708673	121.6305564	-179.7767848	-5.4655090	3.5976340	0.2561570
9	No	9	C	4	3	2	1.4588916	117.7262344	-176.7360038	-4.8280090	-0.9237600	0.4274200

10	No	10	H	5	4	3	1.0679602	118.9188585	-178.6551795	-2.2410420	-0.1341780	0.0864830
11	No	11	C	9	4	3	1.3472996	120.4750457	-1.8086592	-6.1500280	-1.1143090	0.6039790
12	No	12	C	11	9	4	1.4616785	121.7033608	0.2857507	-7.0816290	0.0078280	0.7010990
13	No	13	H	9	4	3	1.0719170	118.9002007	177.2075074	-4.1630900	-1.7597550	0.3379710
14	No	14	H	11	9	4	1.0680710	122.1194268	179.6339148	-6.5792030	-2.0900770	0.6707720
15	No	15	N	6	5	4	1.4286854	118.8626090	-178.7043225	-1.0622770	2.2163110	-0.1772030
16	No	16	O	12	11	9	1.3794750	116.0863620	1.0914885	-6.5302930	1.2663340	0.5780440
17	No	17	O	12	11	9	1.2205621	125.9004876	-179.1035784	-8.2867620	-0.0755110	0.8756870
18	No	18	C	15	6	5	1.2890953	119.9014805	-149.7727331	-0.5081600	3.2920460	0.2672240
19	No	19	H	18	15	6	1.0787986	117.2334829	6.3742891	-1.1129510	3.9419560	0.8801280
20	No	20	C	18	15	6	2.5040848	100.8303384	-163.0470874	1.6180380	3.3071250	-1.0554610
21	No	21	C	20	18	15	1.4143672	29.5993027	-166.8533340	0.8326940	3.7928380	0.0158710
22	No	22	C	21	20	18	1.4530164	119.6499847	-174.3802770	1.3189570	4.9023110	0.8182890
23	No	23	C	22	21	20	1.4193214	120.0858994	3.9633709	2.5352730	5.5486860	0.4758740
24	No	24	C	23	22	21	1.4368225	118.6776741	-1.3102691	3.2789490	5.0646390	-0.6542160
25	No	25	C	24	23	22	1.3509852	121.2993403	-1.0827467	2.8525180	4.0027540	-1.3723510
26	No	26	H	22	21	20	2.1735833	98.3988540	-173.4680074	-0.2372800	4.9027010	2.3357180
27	No	27	C	22	21	20	1.4276935	123.5095114	-174.6194740	0.6496700	5.3853990	1.9831880
28	No	28	C	23	22	21	1.4132853	120.7950236	179.4053384	3.0157980	6.6372340	1.2384580
29	No	29	H	24	23	22	1.0746872	118.4779637	179.7699490	4.1975590	5.5588010	-0.9128900
30	No	30	H	25	24	23	1.0714842	122.2099802	-179.0763469	3.4027980	3.6206920	-2.2085920
31	No	31	C	28	23	22	1.3762011	121.4142528	0.5352175	2.3315420	7.0992590	2.3394830
32	No	32	C	27	22	21	1.3773001	121.8396856	-179.3688695	1.1350640	6.4487880	2.7115780
33	No	33	H	28	23	22	1.0746129	118.4224952	-179.8862656	3.9400890	7.0995810	0.9439850
34	No	34	H	31	28	23	1.0728275	120.9990384	179.7569048	2.7044270	7.9236790	2.9158920
35	No	35	H	32	27	22	1.0737801	119.3057105	-179.6433278	0.6017740	6.7749240	3.5846420
36	No	36	O	20	18	15	1.2978208	95.9823293	6.3681025	1.3153040	2.2952960	-1.8097110
37	No	37	Hg	36	20	18	2.2509819	129.7874342	-41.6629512	0.3246380	0.3458860	-1.2755750
38	No	38	C	37	36	20	3.4763978	84.9448751	-83.0687714	3.5122990	-0.6580630	-0.3183680
39	No	39	C	38	37	36	1.3809363	167.3621337	-37.4458050	4.8657240	-0.8950010	-0.1802150
40	No	40	C	39	38	37	1.3917728	119.4769540	-143.6852553	5.3009840	-2.1382700	0.2690760
41	No	41	C	40	39	38	1.3901211	120.1907775	0.6754938	4.3799160	-3.1372450	0.5625370
42	No	42	C	41	40	39	1.4002044	120.4584552	-0.4687520	3.0071860	-2.9013800	0.4191760
43	No	43	C	42	41	40	1.4224664	121.5243409	-0.3097895	2.5106980	-1.6430470	-0.0207200
44	No	44	H	38	37	36	1.0729000	51.2868259	4.5279882	3.1867750	0.3050860	-0.6611400
45	No	45	H	39	38	37	1.0721100	120.9219054	36.5104979	5.5846580	-0.1339420	-0.4111760
46	No	46	C	41	40	39	1.4547352	116.6797732	178.8953092	4.9195920	-4.4145190	1.0025090
47	No	47	H	42	41	40	1.0698412	119.0282534	177.3997599	2.3205720	-3.6990880	0.6109660
48	No	48	C	46	41	40	1.3478992	121.5370234	0.4951056	6.2467900	-4.6133760	1.1283410
49	No	49	C	48	46	41	1.4660781	121.2158408	0.0143357	7.2068150	-	0.8264820

											3.5472530	
50	No	50	H	46	41	40	1.0732471	118.1817648	-179.4976246	4.2301000	-5.2055740	1.2276580
51	No	51	H	48	46	41	1.0694553	122.9944560	-179.9877937	6.6686470	-5.5421770	1.4494330
52	No	52	N	43	42	41	1.3549651	124.5232013	-179.2156618	1.1971490	-1.3440450	-0.1660380
53	No	53	O	49	48	46	1.3556454	116.2298956	-0.2514346	6.6818840	-2.3675360	0.4135780
54	No	54	O	49	48	46	1.2277086	124.0834076	179.7359446	8.4243200	-3.6689830	0.9271390
55	No	55	C	52	43	42	1.4335352	118.8866820	8.9629590	0.2179370	-2.2719680	0.3188600
56	No	56	H	55	52	43	1.0761186	113.3427234	36.9807252	0.5066570	-2.7564490	1.2353480
57	No	57	C	55	52	43	2.5528744	102.2078313	-141.9653373	-1.5952580	-2.1286170	-1.4724920
58	No	58	C	55	52	43	1.3741585	129.7062862	-144.5091325	-1.0140210	-2.5970940	-0.1958090
59	No	59	C	58	55	52	1.4932951	119.3197874	-175.0693492	-1.9025330	-3.5253430	0.5650000
60	No	60	C	59	58	55	1.4486238	120.2461693	-156.7640289	-2.9347320	-4.2743460	-0.1220740
61	No	61	C	60	59	58	1.3956437	119.8305526	-10.6596501	-3.2489660	-3.9685840	-1.4470600
62	No	62	C	57	55	52	1.3696979	142.4667385	153.5013122	-2.6080910	-2.8453740	-2.0525790
63	No	63	H	59	58	55	2.1406421	95.9166207	25.0468517	-1.0602940	-3.1098650	2.4886320
64	No	64	C	59	58	55	1.4094352	121.8862481	21.8064236	-1.7545000	-3.7280180	1.9519090
65	No	65	C	60	59	58	1.4414320	117.4087267	171.5904979	-3.6325400	-5.2864390	0.6305600
66	No	66	H	61	60	59	1.0752213	120.9167814	179.6167982	-4.0076820	-4.5172670	-1.9756410
67	No	67	H	62	57	55	1.0762120	116.1071020	-160.9582014	-2.9416790	-2.4996090	-3.0155940
68	No	68	C	65	60	59	1.3724255	122.1560376	4.4373223	-3.4082230	-5.4854710	1.9698210
69	No	69	C	64	59	58	1.3899445	123.3904840	-173.5406950	-2.4747850	-4.6773120	2.6674340
70	No	70	H	65	60	59	1.0765668	117.7084178	-176.8903703	-4.3647210	-5.8807430	0.1112240
71	No	71	H	68	65	60	1.0773338	119.8454227	179.1696638	-3.9606310	-6.2440380	2.4990370
72	No	72	H	69	64	59	1.0747413	120.6547591	-179.2221940	-2.3356740	-4.7861300	3.7275640
73	No	73	O	57	55	52	1.3826199	97.9554315	-14.3469473	-1.1589730	-0.9733780	-2.0943570

S12. Physical parameters of the ligand $L+Hg^{2+}$

Sum of Mulliken charges= -2.00000

Electronic spatial extent (au): <R**2>= 36870.3946

Charge= -2.0000 electrons

Dipole moment (field-independent basis, Debye):

X= 2.8965 Y= 16.5155 Z= 1.8719 Tot= 16.8717

Quadrupole moment (field-independent basis, Debye-Ang):

XX= -589.4212 YY= -403.5143 ZZ= -336.1079

XY= 11.3720 XZ= -4.6318 YZ= 2.9316

Traceless Quadrupole moment (field-independent basis, Debye-Ang):

XX= -146.4067 YY= 39.5002 ZZ= 106.9065

XY= 11.3720 XZ= -4.6318 YZ= 2.9316

Octapole moment (field-independent basis, Debye-Ang**2):

XXX= -68.2688 YYY= 268.2737 ZZZ= -182.5448 XYY= 28.2604

XXY= 543.6079 XXZ= -317.3793 XZZ= 49.0840 YZZ= 68.3999

YYZ= -73.3490 XYZ= 5.8736

Hexadecapole moment (field-independent basis, Debye-Ang**3):

XXXX=-48507.4190 YYYY=-24835.5593 ZZZZ= -3056.3848 XXXY= 4199.1679

XXXZ= -111.6962 YYYX= -700.8153 YYYZ= 85.7174 ZZZX= -101.1828

ZZZY= -15.5247 XXYY= -9884.9675 XXZZ= -5445.1212 YYZZ= -4456.5520

XXYZ= 239.7763 YYXZ= -59.4178 ZZXY= -182.7533

N-N= 5.726967235681D+03 E-N=-1.650073956872D+04 KE= 2.118026131083D+03

S13. Various bond lengths, angles and dihedral angles of L +Pb^{2+} generated by HF method

Row	Highlight	Tag	Symbol	NA	NB	NC	Bond	Angle	Dihedral	X	Y	Z
1	No	1	C							-2.0784510	0.2721820	-1.8683550
2	No	2	C	1			1.3879189			-3.4222320	0.4988020	-2.1314420
3	No	3	C	2	1		1.3887601	118.8286005		-4.2350440	0.9684400	-1.1080010
4	No	4	C	3	2	1	1.3949291	121.8068214	-0.4660367	-3.7391660	1.2076970	0.1736730
5	No	5	C	4	3	2	1.3991332	118.9855219	0.6083334	-2.3826730	0.9794100	0.4293790
6	No	6	C	5	4	3	1.3880775	119.6486877	0.3560583	-1.5577180	0.5288780	-0.5920070
7	No	7	H	1	2	3	1.0713439	119.9610994	178.1338364	-1.4413880	-0.1183490	-2.6360880
8	No	8	H	2	1	6	1.0697318	121.6939854	-179.8649964	-3.8459230	0.3095540	-3.0952870
9	No	9	C	4	3	2	1.4590296	117.6335886	-179.2702473	-4.6772710	1.6851060	1.1840230
10	No	10	H	5	4	3	1.0716312	120.3147709	-179.5475721	-1.9806780	1.1492620	1.4081250
11	No	11	C	9	4	3	1.3416225	120.9597538	-0.2998142	-5.9686900	1.8909740	0.8843460
12	No	12	C	11	9	4	1.4714472	121.3213175	-0.0760308	-6.4880090	1.6459960	-0.4704420
13	No	13	H	9	4	3	1.0720412	118.5368211	179.5460396	-4.3131860	1.8666330	2.1758710
14	No	14	H	11	9	4	1.0685713	123.0271111	179.8856659	-6.6840720	2.2380350	1.5982240
15	No	15	N	6	5	4	1.4483277	119.3197195	-179.2278698	-0.1582520	0.2788060	-0.3152180
16	No	16	O	3	2	1	1.3767621	117.8425144	179.8722421	-5.5640490	1.1887430	-1.3920540
17	No	17	O	12	11	9	1.2086551	125.3714755	-179.5635365	-7.6322010	1.8134770	-0.8220410
18	No	18	C	15	6	5	1.2864940	119.0964862	-107.5029258	0.7257120	1.0916290	-0.7767300
19	No	19	H	18	15	6	1.0762130	116.9805106	1.6233835	0.3658280	1.9415070	-1.3302870
20	No	20	C	18	15	6	2.4892160	101.9672030	-165.9175128	2.8289250	-0.2035510	-0.4681850
21	No	21	C	20	18	15	1.3777270	29.9276563	-159.2746732	2.1834130	1.0003610	-0.6471870
22	No	22	C	21	20	18	1.4449460	118.6621800	-177.1779160	2.9777520	2.2010850	-0.7702980

23	No	23	C	22	21	20	1.4178140	118.8492808	1.8998145	4.3911140	2.0920810	-0.7434170
24	No	24	C	23	22	21	1.4233167	119.5100157	-0.8744027	4.9926000	0.8127620	-0.5779240
25	No	25	C	24	23	22	1.3649659	121.2240830	-0.4689008	4.2337250	-0.3127390	-0.4347870
26	No	26	H	22	21	20	2.1784360	98.5225142	-176.2090395	1.3559670	3.6517660	-0.8748040
27	No	27	C	22	21	20	1.4266583	123.4550669	-176.9695294	2.4158480	3.5064290	-0.8955770
28	No	28	C	23	22	21	1.4227498	120.0480387	179.7418103	5.1979990	3.2572470	-0.8680840
29	No	29	H	24	23	22	1.0721247	118.8597052	-179.7734290	6.0622050	0.7428360	-0.5554090
30	No	30	H	25	24	23	1.0700963	121.9255906	-178.9006581	4.6738620	-1.2776830	-0.2924190
31	No	31	C	28	23	22	1.3681342	120.9166250	0.3775997	4.6299420	4.4940780	-1.0071940
32	No	32	C	27	22	21	1.3715262	121.0735009	-179.7248019	3.2167350	4.6133910	-1.0151560
33	No	33	H	28	23	22	1.0725045	118.6709099	-179.9288403	6.2648140	3.1491500	-0.8460250
34	No	34	H	31	28	23	1.0711592	120.7322217	179.8946954	5.2402560	5.3695460	-1.0991430
35	No	35	H	32	27	22	1.0718414	119.6326328	-179.8309315	2.7699730	5.5835150	-1.1051950
36	No	36	O	20	18	15	1.3869313	90.0908950	17.9541155	2.0930170	-1.3720200	-0.3389640
37	No	37	H	36	20	18	1.0036509	117.0473176	110.1187938	2.1578660	-2.0373660	-1.0875790
38	No	38	Pb	36	20	18	2.2948051	127.2720775	-45.3699487	0.1978610	-1.6892680	0.9155750
39	No	39	O	38	36	20	2.8099369	118.5169710	-15.3844614	-0.4503690	0.2196900	2.8729770
40	No	40	O	38	36	20	2.5017467	72.6743648	139.5061309	-0.1288960	-2.9026510	-1.2476790
41	No	41	O	39	38	36	2.2088923	114.8015101	-36.8289165	1.2829590	1.0797060	3.9384120
42	No	42	O	39	38	36	2.1918496	54.7193467	-32.6398047	1.5826240	-0.3404670	2.2751740
43	No	43	O	40	38	36	2.1967861	166.8040390	22.4799460	0.0887750	-3.9605530	-3.1606170
44	No	44	O	43	40	38	2.1972627	60.3908124	-8.7525370	1.8518030	-3.0501450	-2.2167670
45	No	45	N	41	39	38	1.2163109	28.9575793	3.8507858	0.8126740	0.3600000	3.0780240
46	No	46	N	43	40	38	1.2176634	30.3708386	-8.7556955	0.5875110	-3.3296920	-2.2462970

S14. Physical parameters of the ligand $L+Pb^{2+}$

Sum of Mulliken charges= 0.00000

Electronic spatial extent (au): <R**2>= 11625.9944

Charge= 0.0000 electrons

Dipole moment (field-independent basis, Debye):

X= -5.0783 Y= 1.5804 Z= -0.8466 Tot= 5.3855

Quadrupole moment (field-independent basis, Debye-Ang):

XX= -167.5175 YY= -129.9791 ZZ= -134.8556

XY= 6.6617 XZ= -2.6490 YZ= -2.6161

Traceless Quadrupole moment (field-independent basis, Debye-Ang):

XX= -23.4001 YY= 14.1383 ZZ= 9.2618

XY= 6.6617 XZ= -2.6490 YZ= -2.6161

Octapole moment (field-independent basis, Debye-Ang**2):

XXX= -468.8050 YYY= -16.4784 ZZZ= 8.3244 XYY= 7.3174

XXY= 41.2480 XXZ= -46.6094 XZZ= 47.2175 YZZ= 7.5823

YYZ= 0.9191 XYZ= -23.3809

Hexadecapole moment (field-independent basis, Debye-Ang**3):

XXXX=-15678.4650 YYYY= -1819.8038 ZZZZ= -568.0454 XXXY= 160.4176

XXXZ= -27.3360 YYYX= 40.1345 YYYZ= 11.9103 ZZZX= -31.6943

ZZZY= -25.4703 XXYY= -2366.1211 XXZZ= -2318.2821 YYZZ= -385.2082

XXYZ= -30.0951 YYXZ= 24.4943 ZZXY= -4.9634

N-N= 1.773209392887D+03 E-N=-5.994225155793D+03 KE= 1.046634600290D+03